Chemical Geology 322–323 (2012) 151–171

Contents lists available at SciVerse ScienceDirect

Chemical Geology

journal homepage: www.elsevier.com/locate/chemgeo

A thermodynamic model for predicting mineral reactivity in supercritical carbon dioxide: I. Phase behavior of carbon dioxide–water–chloride salt systems across the H_2O-rich to the CO_2-rich regions

Ronald D. Springer [a], Zheming Wang [b], Andrzej Anderko [a,*], Peiming Wang [a], Andrew R. Felmy [b]

[a] OLI Systems Inc., 108 The American Rd., Morris Plains, NJ 07950, USA
[b] Pacific Northwest National Laboratory, 902 Battelle Blvd, Richland, WA 99352, USA

ARTICLE INFO

Article history:
Received 22 March 2012
Received in revised form 4 July 2012
Accepted 7 July 2012
Available online 15 July 2012

Editor: J. Fein

Keywords:
Supercritical carbon dioxide
Chloride salts
Thermodynamic modeling
Mixed-solvent electrolyte model
Mineral reactivity

ABSTRACT

Phase equilibria in mixtures containing carbon dioxide, water, and chloride salts have been investigated using a combination of solubility measurements and thermodynamic modeling. The solubility of water in the CO_2-rich phase of ternary mixtures of CO_2, H_2O and NaCl or $CaCl_2$ was determined, using near infrared spectroscopy, at 90 atm and 40 to 100 °C. These measurements fill a gap in the experimental database for CO_2–water–salt systems, for which phase composition data have been available only for the H_2O-rich phases. A thermodynamic model for CO_2–water–salt systems has been constructed on the basis of the previously developed Mixed-Solvent Electrolyte (MSE) framework, which is capable of modeling aqueous solutions over broad ranges of temperature and pressure, is valid to high electrolyte concentrations, treats mixed-phase systems (with both $scCO_2$ and water present) and can predict the thermodynamic properties of dry and partially water-saturated supercritical CO_2 over broad ranges of temperature and pressure. Within the MSE framework the standard-state properties are calculated from the Helgeson–Kirkham–Flowers equation of state whereas the excess Gibbs energy includes a long-range electrostatic interaction term expressed by a Pitzer–Debye–Hückel equation, a virial coefficient-type term for interactions between ions and a short-range term for interactions involving neutral molecules. The parameters of the MSE model have been evaluated using literature data for both the H_2O-rich and CO_2-rich phases in the CO_2–H_2O binary and for the H_2O-rich phase in the CO_2–H_2O–NaCl/KCl/$CaCl_2$/$MgCl_2$ ternary and multicompontent systems. The model accurately represents the properties of these systems at temperatures from 0 °C to 300 °C and pressures up to ~4000 atm. Further, the solubilities of H_2O in CO_2-rich phases that are predicted by the model are in agreement with the new measurements for the CO_2–H_2O–NaCl and CO_2–H_2O–$CaCl_2$ systems even though the new data were not used in the parameterization of the model. Thus, the model can be used to predict the effect of various salts on the water content and water activity in CO_2-rich phases on the basis of parameters determined from the properties of aqueous systems. Given the importance of water activity in CO_2-rich phases for mineral reactivity, the model can be used as a foundation for predicting mineral transformations across the entire CO_2/H_2O composition range from aqueous solution to anhydrous $scCO_2$. An example application using the model is presented which involves the transformation of forsterite to nesquehonite as a function of temperature and water content in the CO_2-rich phase.

1. Introduction

Capture and storage of carbon dioxide in geologic formations represents one of the most promising options for mitigating the impact of greenhouse gases on global warming, owing to the potentially large capacity of these formations and their broad regional availability (Bachu, 2002; Bachu and Adams, 2003; Benson and Surles, 2006; Bachu, 2008). As a result, it is important to predict the interactions of carbon dioxide with mineral phases as they relate to geologic disposal of CO_2 and the development of mineral carbonation technologies. This can be a daunting challenge given that carbon dioxide could be a supercritical fluid ($T > 31.1$ °C and $P > 72.9$ atm) (Regnault et al., 2005; Garcia et al., 2010), high partial pressures of carbon dioxide can result in significant formation of carbonic acid (Giammar et al., 2005; Suto et al., 2007; King et al., 2010), and H_2O dissolved in supercritical CO_2 can be highly reactive (Regnault et al., 2005; Kwak et al., 2010, 2011). Although the reactivity of CO_2-containing aqueous solutions, hereafter termed the water-rich phase, is well documented (Giammar et al., 2005; Regnault et al., 2005; Hanchen et al., 2006; Lin et al., 2008; Prigiobbe et al., 2009; Garcia et al., 2010; King et al., 2010; Daval et al., 2011; Guyot et al., 2011), the reactivity of H_2O dissolved in $scCO_2$, hereafter termed the

* Corresponding author. Tel.: +1 973 539 4996x25; fax: +1 973 539 5922.
E-mail address: aanderko@olisystems.com (A. Anderko).

0009-2541/$ – see front matter © 2012 Elsevier B.V. All rights reserved.
doi:10.1016/j.chemgeo.2012.07.008

CO_2-rich phase, has been largely ignored (McGrail et al., 2009; Kwak et al., 2010, 2011). The importance of H_2O reactivity in the CO_2-rich phase results from several factors. First, although the solubility of H_2O in $scCO_2$ is low (<1% by mass) the total chemical potential of H_2O in the CO_2-rich phase will be the same as that of H_2O in the water-rich phase if they are in equilibrium (thermodynamic phase equilibrium condition). In addition, $scCO_2$ is highly diffusive owing to its low viscosity. Hence, in geologic disposal, the $scCO_2$-rich phase is likely to permeate the overlying repository cap rock pore network (Nordbotten and Celia, 2006) enhancing the importance of the reactivity of the CO_2-rich phase in geologic systems. In addition, the migrating $scCO_2$, which initially can be anhydrous, has the potential to extract water from the formation, increasing the electrolyte concentration of the remaining water-rich phase. As a result, in order to model the full range of mineral reactivity related to both the disposal of $scCO_2$ in geologic systems and the development of mineral carbonation technologies, a thermodynamic approach is necessary that can accurately represent the chemical equilibria in both the water-rich and the CO_2-rich phases over broad ranges of temperature, pressure, and electrolyte composition.

In view of the importance of the CO_2–water–salt systems in geochemistry and chemical and petroleum engineering, various computational models have been developed to represent the properties of such systems. In general, these models fall into two distinct categories:

(1) γ–φ models, in which an activity coefficient formulation is used to reproduce the behavior of aqueous solutions whereas an equation of state provides the fugacity coefficients of components in the gas phase and
(2) φ–φ models, in which a homogeneous equation of state is used to reproduce the properties of both the liquid and gas phases.

The existing γ–φ models are focused primarily on reproducing the solubility of CO_2 in water and aqueous solutions of selected salts. In particular, Barta and Bradley (1985), Rumpf et al. (1994), Duan and Sun (2003), Duan et al. (2006) and Akinfiev and Diamond (2010) developed CO_2 solubility models using the well-known Pitzer (1973) activity coefficient formulation for the aqueous phase. Alternatively, the scaled particle theory of electrolyte effects was used by Li and Nghiem (1986). Spycher and Pruess (2005) presented a model for calculating the mutual solubilities of the aqueous and CO_2 phases using the Pitzer (1973) activity coefficients. Salari et al. (2011) developed a model for estimating the water content of CO_2 phases. Furthermore, the γ–φ methods have been combined with speciation calculations by Li and Duan (2007) and Li and Duan (2011).

The φ–φ approaches have been constructed either by incorporating electrolyte-specific terms into nonelectrolyte equations of state or by combining a classical equation of state with an excess Gibbs energy model for electrolytes. The former approach was adopted by Jin and Donohue (1988), Harvey and Prausnitz (1989) and Ji et al. (2005) using the mean spherical approximation theory to account for electrostatic interactions of ions. Tan et al. (2008) reviewed models of this type that are based on the SAFT (Statistical Associating Fluid Theory) equation of state whereas Lin et al. (2007) reviewed those based on cubic and other equations of state. In an alternative approach, Li et al. (2001) and Kiepe et al. (2002) combined a cubic equation of state with a group contribution-based activity coefficient model for electrolytes. Additionally, the φ–φ approaches have been shown to be most appropriate for high-temperature systems (i.e., above ca. 300 °C), in which electrolytes exist primarily in the form of ion pairs (Anderko and Pitzer (1993), Duan et al. (2003)).

The γ–φ and φ–φ approaches have their advantages and disadvantages. In principle, the φ–φ approach is more appropriate for systems that transition from the subcritical to supercritical range because it can handle the vapor-liquid critical behavior, at least within the limitations of classical equations of state. Also, it can reproduce volumetric properties simultaneously with phase equilibria. However, it is much more computationally intensive because the solution of phase equilibrium conditions must be accompanied by solving the equation of state in each phase. The γ–φ methods, while much less computationally intensive, impose a division of the phase space into gas-like and liquid-like regions even when such a division is not physically rigorous. However, the γ–φ methods are much more amenable to integration with speciation and chemical equilibrium calculations. This is particularly important for modeling the interactions between minerals and CO_2-bearing fluid phases, which is the ultimate objective of this work. Therefore, the γ–φ approach is more appropriate here.

The main thrust of this study is to develop a model that not only predicts the solubility of CO_2 in water-rich phases and of water in CO_2-rich phases but can also be used to calculate chemical equilibria involving CO_2-rich phases. This requires developing a thermodynamic model that can handle (1) aqueous solutions over broad ranges of temperature and pressure up to the high electrolyte concentrations found in subsurface brines, and (2) mixed-phase systems (with both $scCO_2$ and water present) that range from dry to partially water-saturated $scCO_2$ over wide ranges of temperature and pressure and include high electrolyte concentrations, which can occur when anhydrous CO_2 is disposed of and acquires water from the formation. Another requirement is the generality of the model and the ease of its extension to multicomponent systems containing multiple solutes and solid phases in the presence of one or two liquid phases and/or a gas phase. These requirements are satisfied by the previously developed Mixed-Solvent Electrolyte (MSE) model (Wang et al., 2002), which has been designed in the γ–φ framework for the simultaneous calculation of phase and chemical equilibria in systems containing strong and weak electrolytes in aqueous, non-aqueous and mixed solvents. This model has been shown to be applicable to mixtures ranging from infinite dilution to the fused salt limit over wide ranges of temperatures (Anderko et al., 2002; Wang et al., 2004, 2006; Gruszkiewicz et al., 2007; Kosinski et al., 2007; Wang et al., 2010). The use of a mole fraction basis within MSE (rather than molality) also allows the mathematical algorithm for solving the phase and chemical equilibrium equations to be stable at the very high concentrations which can occur as electrolyte solutions dry in contact with anhydrous $scCO_2$.

In this contribution, we extend the MSE model to CO_2-dominated systems at high chloride concentrations, temperatures and pressures that are of importance in the disposal of $scCO_2$ in subsurface systems as well as in optimizing the overall mineral carbonation process in industrial systems (Hanchen et al., 2008; Zhao et al., 2010; Guyot et al., 2011). We also present new measurements of H_2O concentrations in $scCO_2$-rich phases that are in equilibrium with aqueous solutions containing variable NaCl and $CaCl_2$ amounts. These measurements provide a stringent test of the validity of the thermodynamic model, which is intended to span the H_2O-rich and CO_2-rich regions. Chloride-containing systems have been chosen for the initial model development since chloride is a primary contributor to expected brine compositions in natural systems (Duan et al., 1995; Duan and Sun, 2003; Spycher and Pruess, 2005). The MSE model parameters for the H_2O-rich phase are developed on the basis of the existing solubility data in chloride-containing systems as well as the mutual solubilities in the CO_2–H_2O binary system over a broad range of CO_2 partial pressures. Thus, the model for the CO_2-rich phase is anchored by the H_2O solubility data in CO_2 and the effect of chloride salts is evaluated from the properties of the H_2O-rich phases, for which relatively abundant experimental data are available. Then, the performance of the model is evaluated against new measurements, performed as part of this study, of the solubility of H_2O in $scCO_2$ in the presence of concentrated NaCl and $CaCl_2$ brines. Finally, an example application is given involving thermodynamic predictions for the transformation of forsterite to nesquehonite in variably wet $scCO_2$, illustrating the importance of modeling the interactions of silicates and the CO_2-rich phase even at low water content.

2. Experimental methods

$CaCl_2 \cdot 2H_2O$, ACS Reagent grade, was purchased from Aldrich. NaCl, Sigma Ultra, minimum 99.5%, was purchased from Sigma. Both reagents were used without further purification. Distilled deionized (DDI) water was generated using a Millipore water filtering system. SFC grade liquid CO_2 was purchased from Matheson Tri-Gas.

All experiments were performed using a modified 160 ml Parr Instruments Series 4793 GP high pressure–high temperature reaction vessel fitted with custom-made 1″ thick ¾″ x 4″ fused silica optical windows. The reaction vessel was pressurized using an ISCO model 260D syringe pump. Multiple two-way valves and a bleeding valve were built into the system to allow the vessel to be pressurized and depressurized without back-flow to the CO_2 supply line along with an in-line rupture disk (Fike Corporation) for safety. The pressure and temperature conditions of the system were monitored using an in-line pressure transmitter (Druck model PTX 500) and four T-type thermocouples (Newport) located at different positions inside the reactor to allow accurate reading of the cell temperature. All the temperature and pressure sensors were interfaced to a 16-bit A/D converter (Measurement Computing model PCI-DAS1602/16) mounted in a personal computer that displayed and recorded temperature and pressure data at 32 Hz. A magnetic stir bar was placed at the bottom of the vessel and a home-made stirrer was placed beneath the reactor to aid mixing of water and $scCO_2$.

Near-infrared (NIR) spectra were measured with a Bruker IFS66 spectrometer equipped with a glow bar and DTG detector for mid-IR and a tungsten light source and a silicon diode detector for NIR spectra range. Spectra were recorded over the range 5000–12,000 cm^{-1} with a resolution of 4 cm^{-1}. The interferometer was scanned at a rate of 1.00 cm/s, and 32 scans were co-added for each spectrum. For spectral acquisition under a specific set of experimental conditions, the reactor was purged with dry N_2 for at least 30 min at the desired temperature and a background spectrum was recorded. After introduction of the aqueous solution placed at the bottom of the reaction vessel, the cell lid was closed and tightened immediately to avoid loss of water vapor. Cell pressurization with $scCO_2$ was initiated and sample spectrum was recorded every 15 min automatically. To avoid over-pressurization, the cell pressurization with $scCO_2$ was carried out with small pressure increments above 1200 psi, allowing $scCO_2$ thermal equilibration with the reactor. The $scCO_2$-water/salt solution mixture was mildly stirred initially for a minimum of 30 min to aid water dissolution. Spectral acquisition was ended when the reaction cell reaches temperature/pressure equilibrium and the spectra were stabilized for the duration of at least an hour.

The presented spectra are the average of a minimum of three consecutive spectra after spectral stabilization. After baseline corrections, the average absorbance of the NIR spectra in the range from 7100 to 7500 cm^{-1} was used to calculate the dissolved water concentrations.

3. Thermodynamic model

3.1. Computational framework

The derivation of the Mixed-Solvent Electrolyte (MSE) thermodynamic framework was described in previous studies (Wang et al., 2002, 2006). In order to apply it to CO_2-containing systems over wide ranges of pressure and temperature, we modify the MSE model by introducing pressure dependence into selected interaction parameters in the activity coefficient formulation. In this section, we briefly summarize the model and define the parameters that need to be evaluated on the basis of experimental data.

In the MSE model, the chemical potential of a species i in a liquid phase is calculated as

$$\mu_i^L = \mu_i^{L,0,x}(T,P) + RT\ln x_i\gamma_i^{x,*}(T,P,\mathbf{x}) \tag{1}$$

where $\mu_i^{L,0,x}(T, P)$ is the standard-state chemical potential expressed on the mole fraction basis, x_i is the mole fraction, and $\gamma_i^{x,*}(T, P, \mathbf{x})$ is the unsymmetrically normalized, mole fraction-based activity coefficient. The mole fraction-based standard-state chemical potential is related to the well-known molality-based standard-state chemical potential by (Wang et al., 2002):

$$\mu_i^{L,0,x}(T,P) = \mu_i^{L,0,m}(T,P) + RT\ln\frac{1000}{M_{H_2O}} \tag{2}$$

where M_{H_2O} is the molecular weight of water. The molality-based standard-state chemical potential is calculated as a function of temperature and pressure from the Helgeson–Kirkham–Flowers (HKF) equation of state (Helgeson et al., 1974a, 1974b, 1976, 1981; Tanger and Helgeson, 1988). The parameters of the HKF equation are available for various species from Shock and Helgeson (1988), Shock et al. (1989), and Johnson et al. (1992). For water, the standard-state chemical potential is defined as that of pure water and is calculated from the Haar–Gallagher–Kell equation of state (Haar et al., 1984).

The activity coefficients in Eq. (1) are obtained from an expression for the excess Gibbs energy, which is expressed as a sum of three contributions:

$$\frac{G^{ex}}{RT} = \frac{G^{ex}_{LR}}{RT} + \frac{G^{ex}_{II}}{RT} + \frac{G^{ex}_{SR}}{RT} \tag{3}$$

where G^{ex}_{LR} represents the contribution of long-range electrostatic interactions, G^{ex}_{II} accounts for specific ionic (ion-ion and ion-molecule) interactions, and G^{ex}_{SR} is a short-range contribution resulting from intermolecular interactions. The long-range interaction contribution is calculated from the Pitzer–Debye–Hückel formula (Pitzer, 1980) expressed in terms of mole fractions and symmetrically normalized, *i.e.*,

$$\frac{G^{ex}_{LR}}{RT} = -\left(\sum_i n_i\right)\frac{4A_xI_x}{\rho}\ln\left(\frac{1+\rho I_x^{1/2}}{\sum_i x_i\left[1+\rho\left(I^0_{x,i}\right)^{1/2}\right]}\right) \tag{4}$$

where the sum is over all species, I_x is the mole fraction-based ionic strength, $I^0_{x,i}$ is defined as the ionic strength in the limiting case when $x_i = 1$, *i.e.*, $I^0_{x,i} = 0.5z_i^2$; ρ is assigned a universal dimensionless value ($\rho = 14.0$), and A_x is given by

$$A_x = \frac{1}{3}(2\pi N_A d_s)^{1/2}\left(\frac{e^2}{4\pi\varepsilon_0\varepsilon_s k_B T}\right)^{3/2} \tag{5}$$

where d_s and ε_s are the molar density and dielectric constant of the solvent, respectively.

The specific ion-interaction contribution is calculated from an ionic strength-dependent, symmetrical second virial coefficient-type expression (Wang et al., 2002):

$$\frac{G^{ex}_{II}}{RT} = -\left(\sum_i n_i\right)\sum_i\sum_j x_ix_jB_{ij}(I_x) \tag{6}$$

where $B_{ij}(I_x) = B_{ji}(I_x)$, $B_{ii} = B_{jj} = 0$, and the ionic strength dependence of B_{ij} is given by

$$B_{ij}(I_x) = b_{ij} + c_{ij}\exp\left(-\sqrt{I_x + a_1}\right) \tag{7}$$

where b_{ij} and c_{ij} are binary interaction parameters and a_1 is set equal to 0.01. The parameters b_{ij} and c_{ij} are calculated as functions of temperature as

$$b_{ij} = b_{0,ij} + b_{1,ij}T + b_{2,ij}/T + b_{3,ij}T^2 + b_{4,ij}\ln T \tag{8}$$

$$c_{ij} = c_{0,ij} + c_{1,ij}T + c_{2,ij}/T + c_{3,ij}T^2 + c_{4,ij}\ln T \tag{9}$$

The coefficients $b_{k,ij}$ (k = 0, …, 4) and $c_{k,ij}$ (k = 0, …, 4) are obtained from the regression of experimental data. For the majority of species pairs, *i*–*j*, the full complexity of the temperature dependence of b_{ij} and c_{ij} in Eqs. (8) and (9) is not needed, and only a limited number of coefficients are used.

The short-range interaction contribution is calculated from the UNIQUAC equation (Abrams and Prausnitz, 1975):

$$\frac{G^{ex}_{SR}}{RT} = \left(\sum_i n_i\right)\left[\sum_i x_i \ln\frac{\varphi_i}{x_i} + \frac{Z}{2}\sum_i q_i x_i \ln\frac{\theta_i}{\varphi_i}\right] - \left(\sum_i n_i\right)\left[\sum_i q_i x_i \ln\left(\sum_j \theta_j \tau_{ij}\right)\right] \tag{10}$$

θ_i, φ_i, and τ_i are defined as

$$\theta_i = \frac{q_i x_i}{\sum_j q_j x_j} \tag{11}$$

$$\varphi_i = \frac{r_i x_i}{\sum_j r_j x_j} \tag{12}$$

$$\tau_{ji} = \exp\left(-\frac{a_{ji}}{RT}\right) \tag{13}$$

where q_i and r_i are the surface and size parameters, respectively, for the species *i*, *Z* is a fixed coordination number ($Z = 10$), and a_{ij} is the binary interaction parameter between species *i* and *j* ($a_{ij} \neq a_{ji}$). The short-range interaction parameters are calculated as functions of temperature and pressure by

$$a_{ij} = a_{ij}^{(0)} + a_{ij}^{(1)}T + a_{ij}^{(2)}T^2 + \left(a_{ij}^{(P0)} + a_{ij}^{(P1)}T + a_{ij}^{(P2)}T^2\right)P \tag{14}$$

where $a_{ij} \neq a_{ji}$. As with the ionic interaction parameters, all coefficients of Eq. (14) are usually not needed for most species pairs. In systems containing only strong electrolytes, only the ion interaction parameters (Eqs. (8)–(9)) are needed. The short-range parameters (Eq. (14)) are introduced only for interactions involving neutral molecules.

The activity coefficients are calculated from Eq. (3) by differentiation with respect to the number of moles (Pitzer, 1995). Since the activity coefficients calculated from Eq. (3) are symmetrically normalized (i.e., they are equal to 1 for each pure component), they need to be converted to unsymmetrical normalization so that they are based on the infinite-dilution reference state in water and can be used in Eq. (1):

$$\ln\gamma_i^{x,*} = \ln\gamma_i^{x} - \lim_{\substack{x_i\to 0 \\ x_w\to 1}} \ln\gamma_i^{x} \tag{15}$$

where $\lim_{\substack{x_i\to 0 \\ x_w\to 1}} \ln\gamma_i^{x}$ is the value of the symmetrically-normalized activity coefficient at infinite dilution in water, which is calculated by substituting $x_i = 0$ and $x_w = 1$ into the activity coefficient equations.

The chemical potential of species *i* in the gas phase is given by

$$\mu_i^G = \mu_i^{G,0}(T) + RT\ln\frac{Py_i\phi_i(T,P)}{P^0} \tag{16}$$

where $\mu_i^{G,0}(T)$ is the chemical potential of pure component *i* in the ideal gas state, y_i is the mole fraction in the gas phase, $\phi_i(T, P)$ is the fugacity coefficient, *P* is the total pressure, and $P^0 = 1$ atm. The $\mu_i^{G,0}(T)$ term is calculated from the ideal-gas Gibbs energy of formation, entropy and heat capacity according to standard thermodynamics (Pitzer, 1995). For water, this term is obtained from the Haar–Gallagher–Kell equation of state (Haar et al., 1984). The fugacity coefficient is calculated from the Soave–Redlich–Kwong (SRK) equation of state (Soave, 1972):

$$P = \frac{RT}{v-b} - \frac{a}{v(v+b)} \tag{17}$$

where *v* is the molar volume and the parameters *a* and *b* are calculated using the classical quadratic mixing rules, i.e.,

$$a = \sum_i \sum_j x_i x_j \left(a_i a_j\right)^{1/2}\left(1-k_{ij}\right) \tag{18}$$

$$b = \sum_i x_i b_i \tag{19}$$

The pure-component parameters a_i and b_i are calculated using the critical properties T_c and P_c and a temperature-dependent function $\alpha(T)$, which is regressed to match pure-component vapor pressures:

$$a_i = 0.42747\frac{R^2T_{ci}^2}{P_{ci}}\alpha_i(T) \tag{20}$$

$$b_i = 0.08664\frac{RT_{ci}}{P_{ci}} \tag{21}$$

The binary parameter k_{ij} in Eq. (18) is expressed as a function of temperature as

$$k_{ij} = k_{ij}^{(0)} + k_{ij}^{(1)}/T \tag{22}$$

The fugacity coefficient $\phi_i(T, P)$ is calculated from Eqs. (17)–(22) using standard thermodynamic relations (Pitzer, 1995).

The expressions for the chemical potentials of species in the liquid and gas phases are further used for the simultaneous calculation of phase (i.e., vapor-liquid and liquid-liquid) equilibria and chemical (or speciation) equilibria between solution species as described by Zemaitis et al. (1986) and Rafal et al. (1995). The calculations were performed using a phase and chemical equilibrium algorithm that is implemented in the OLI software (OLISystems, 2012). The model parameters reported here are available in the OLI software starting from version 9.0.

3.2. Determination of model parameters

The combined thermodynamic framework has been applied to model the phase behavior of binary and mixed CO_2–Na–K–Mg–Ca–Cl–H_2O systems. Table 1 summarizes the available literature sources for these systems together with their temperature, pressure, and salt content ranges.

For the binary and multicomponent Na–K–Mg–Ca–Cl–H_2O systems (i.e., without CO_2), the MSE parameters were determined in a previous study (Gruszkiewicz et al., 2007). These parameters ensure that the model reproduces the phase equilibria and caloric properties of binary, ternary, and multicomponent mixtures from the freezing point up to 300 °C and from infinite dilution to the solid saturation or fused salt limit. Table 2 summarizes the parameters that determine the thermodynamic properties of individual species in the Na–K–Mg–Ca–Cl–H_2O systems (i.e., the standard partial molar Gibbs energy of formation, entropy, and parameters of the HKF equation of state). These species include the individual ions (i.e., Na^+, K^+, Mg^{2+}, Ca^{2+}, and Cl^-) and the ion pairs (i.e., $MgCl_{2(aq)}$ and $CaCl_{2(aq)}$) that were taken into account in the previous study (Gruszkiewicz et al., 2007). Table 3 compiles the ionic interaction parameters (Eqs. (8)–(9)) between these species.

In this study, we determine parameters to reproduce the properties of the following systems:

(1) The binary system CO_2–H_2O
(2) Ternary mixtures composed of CO_2, H_2O and one of the four chloride salts, i.e., NaCl, KCl, $MgCl_2$, and $CaCl_2$
(3) Multicomponent mixtures containing CO_2, H_2O and various combinations of NaCl, KCl, $MgCl_2$ or $CaCl_2$.

In the first step of model development, MSE parameters have been determined for the CO_2–H_2O binary. There are a large number of experimental studies that report experimental data for this system (cf. Table 1). Furthermore, critical reviews are available to guide the relative weighting of experimental data for model development. The data that are available in the low-pressure range and at temperatures up to 433 K have been reviewed by Carroll et al. (1991). The solubilities of CO_2 in H_2O have been evaluated by Crovetto (1991) at temperatures up to the critical point, by Diamond and Akinfiev (2003) up to 100 °C and 100 MPa and by Duan and Sun (2003) up to 260 °C and 200 MPa. Spycher et al. (2003) reviewed the mutual solubilities of CO_2 and H_2O up to 100 °C and 60 MPa. The latter three reviews deal with the conditions that are particularly relevant to geological sequestration. The data at higher temperatures and pressures have been evaluated by Mäder (1991), Mather and Franck (1992) and Blencoe et al. (2001).

In this study, we regress parameters to reproduce the experimental data for temperatures ranging from 0 °C to 300 °C and pressures up to approximately 350 MPa. The parameters are determined on the basis of (a) solubilities of CO_2 in H_2O, (b) solubilities of H_2O in CO_2, (c) pure-component vapor-pressures of CO_2 and (d) enthalpies of mixing of CO_2 and H_2O. The application of the MSE model to the CO_2–H_2O system is constrained by the inherent characteristics of the γ–φ methods for calculating phase equilibria (Anderko and Malanowski, 1992). In the γ–φ methods, fluid phase equilibria can be calculated as either vapor-liquid (VLE) or liquid-liquid (LLE) equilibria. In the former case, the model uses separate formulations for the two phases, i.e., Eq. (1) for the liquid phase and Eq. (16) for the vapor phase. In the latter case, Eq. (1) is used for both phases. Below the critical temperature of the lighter component (i.e., below 304.12 K in the case of CO_2), there is a distinct transition between the VLE and LLE regions. The two regions are separated by the three-phase vapor–liquid–liquid region and the three-phase equilibrium pressure is, at a given temperature, very close to the vapor pressure of pure CO_2. Above the critical temperature of CO_2, there is only one fluid-fluid equilibrium region, which transitions smoothly from a VLE-like region to an LLE-like region as the pressure increases. However, a γ–φ model still calculates phase equilibria as VLE at lower pressures and as LLE at higher pressures. The transition between these two regions becomes then arbitrary and lies on an extension of the VLLE P vs. T curve beyond the critical temperature of CO_2. However, with appropriately adjusted model parameters, the VLE-like and LLE-like regions can merge seamlessly and correctly approximate the solubility of $scCO_2$ in the water phase and water in the $scCO_2$ phase across the full pressure range of phase equilibria.

In order to reproduce the behavior of the CO_2–H_2O binary, the MSE model requires three kinds of parameters, i.e., (1) the standard-state Gibbs energy of formation, entropy and HKF equation parameters for $CO_{2(aq)}$, (2) the interaction parameters in the formulation for the excess Gibbs energy (Eqs. (8) and (14)) and (3) standard-state properties of CO_2 in the gas phase and the parameters of the SRK equation (Eqs. (17)–(22)). In the LLE region of the phase coexistence curve, the properties of both phases are modeled using the liquid-phase chemical potential expression (Eq. (1)). Thus, the LLE region is reproduced exclusively by the liquid-phase interaction parameters because the standard-state chemical potential drops out when Eq. (1) is applied to both coexisting phases. On the other hand, the VLE region is represented by Eq. (1) for the liquid phase and Eq. (16) for the gas phase. The liquid-phase properties in the VLE region depend primarily on the standard-state properties and, to a lesser extent, on the liquid-phase interaction parameters. The liquid-phase interaction parameters play a much lesser role here because the concentration of CO_2 in the water-rich phase is relatively low. The chemical potential of CO_2 in the gas phase depends on the SRK interaction parameters (Eq. (22)) in addition to the pure-component properties, which are fixed at their experimental values and collected in Table 4. At low pressures, the gas phase is nearly ideal and VLE calculations depend primarily on the standard-state properties of $CO_{2(aq)}$. As the pressure increases, the gas-phase fugacity coefficients increasingly depend on the SRK interaction coefficients. In view of the different sensitivity of the VLE and LLE regions to various model parameters, initial estimates of the liquid-phase interaction parameters (Eqs. (8) and (14)) have been obtained from the data in the LLE region whereas the initial values of the SRK interaction parameters (Eq. (22)) have been obtained from the VLE region in the elevated pressure range. Subsequently, the parameters have been refined through a combined optimization using a complete set of phase equilibrium data. For the liquid-phase interaction parameters, it has been determined that the optimum representation of phase equilibria is obtained using the ionic strength-independent virial parameters B_{ij} in the virial expansion (i.e., by using only the coefficients $b_{0,ij}$, $b_{1,ij}$, and $b_{2,ij}$ in Eq. (8) and setting all c_{ij} coefficients in Eq. (9) equal to zero) coupled with the pressure-dependent UNIQUAC interaction parameters a_{ij} (i.e., by regressing the coefficients $a_{ij}^{(0)}$, $a_{ij}^{(1)}$, $a_{ij}^{(P0)}$, and $a_{ij}^{(P1)}$ in Eq. (14), the last two of which impose a linear pressure dependence on a_{ij}). The pressure dependence is necessary due to the very wide pressure range of the available phase equilibrium data (up to 350 MPa). For simplicity and in view of the rather small differences in the sizes of the species considered here, the r_i and q_i parameters in the short-range term (Eqs. (11)–(12)) are set equal to 0.92 and 1.4, respectively, for all species. The HKF equation parameters for $CO_{2(aq)}$ have been slightly adjusted by modifying the $a_{HKF,1,\ldots4}$ parameters in the combined model while keeping the remaining parameters (i.e., $c_{HKF,1}$, $c_{HKF,2}$ and ω) unchanged. Table 2 includes the standard-state properties of $CO_{2(aq)}$. The virial-type interaction parameters between CO_2 and H_2O ($b_{0,ij}$, $b_{1,ij}$, and $b_{2,ij}$) are listed in Table 3. Finally, Table 5 contains the UNIQUAC liquid-phase interaction parameters ($a_{ij}^{(0)}$, $a_{ij}^{(1)}$, $a_{ij}^{(P0)}$, and $a_{ij}^{(P1)}$) and the SRK binary parameters ($k_{ij}^{(0)}$ and $k_{ij}^{(0)}$).

In the second stage of parameter development, mixtures containing chloride salts as well as CO_2 and H_2O have been analyzed. Table 1 summarizes the sources of experimental data that include NaCl, KCl, $MgCl_2$, and $CaCl_2$ as the salt components and lists the temperature, pressure and salt content ranges of the data. The experimental data base is particularly abundant in the case of NaCl–CO_2–H_2O system, for which 27 data sources have been identified. For this system, the experimental studies have been reviewed by Spycher and Pruess (2005) and Koschel et al. (2006). The data are also fairly extensive for the KCl–CO_2–H_2O and $CaCl_2$–CO_2–H_2O systems, for each of which 11 data sources are available. For these three ternary systems, a significant number of data sets extend well into the temperature and pressure ranges that are relevant to CO_2 sequestration (cf. Table 1). Data for the $MgCl_2$–CO_2–H_2O system are limited to a small number of sources (i.e., three) and ambient pressures. Only a few data sets are available for mixed chloride salts. It should be noted that all of the literature data sources pertain to the water-rich liquid phase and none of them deals with the carbon dioxide-rich phase in the presence of salts.

Analysis of experimental data has revealed that the effect of salts on the solubility of CO_2 can be reproduced using a single, temperature-independent interaction parameter $b_{0,ij}$ between the cations (i.e., Na^+, K^+, Mg^{2+} and Ca^{2+}) and $CO_{2(aq)}$ in the virial term (Eq. (8)). These parameters are listed in Table 3. Considering the wide temperature, pressure and salt concentration ranges of

Table 1
Experimental data sources for the CO_2–Na–K– Mg–Ca–Cl–H_2O systems.

System	Reference	Temperature range, K	Pressure range, atm	Salt concentration mol·kg^{-1} H_2O
CO_2–H_2O	Bunsen (1855b)	277.55–295.55	1	0
	Bunsen (1855a)	273.15–293.15	1	0
	de Khanikof and Louguinine (1867)	288.15	1–4	0
	Setschenow (1874)	288.35–290.25	1	0
	Setchenow (1879)	310.4	1	0
	Setchenow (1887)	288.35–296.15	1	0
	Setchenow (1889)	288.35	1	0
	Bohr and Bock (1891)	310.44–373.15	1	0
	Setchenow (1892)	288.35	1	0
	Prytz and Holst (1895)	273.15	1	0
	Bohr (1899)	273.25–334.55	1	0
	Hantzsch and Vogt (1901)	273.15–363.15	0.09–0.12	0
	Geffcken (1904)	288.15–298.15	1	0
	Findlay and Creighton (1910)	298.15	1–1.8	0
	Findlay and Shen (1912)	298.15	1–1.8	0
	Sander (1912)	293.15–375.15	25–165	0
	Findlay and Williams (1913)	298.15	0.35–1	0
	Findlay and Howell (1915)	298.15	0.35–1.3	0
	Kunerth (1922)	293.15–307.15	1	0
	Morgan and Pyne (1930)	298.15	1	0
	Morgan and Maass (1931)	273.15–298.15	0.1–1.1	0
	Kritschewski et al. (1935)	293.15–303.15	5–30	0
	Kobe and Williams (1935)	298.15	1	0
	Shedlovsky and MacInnes (1935)	298.15	1	0
	Zelvenskii (1937)	273.15–373.15	10–95	0
	Curry and Hazelton (1938)	298.15	1	0
	Van Slyke (1939)	295.95–298.65	1	0
	Wiebe and Gaddy (1939)	323.15–373.15	25–700	0
	Wiebe and Gaddy (1940)	285.15–313.15	25–500	0
	Markham and Kobe (1941)	273.35–313.15	1	0
	Wiebe and Gaddy (1941)	298.15	500	0
	Harned and Davis (1943)	273.15–323.15	1	0
	Stone (1943)	244.15–295.75	15–60	0
	Prutton and Savage (1945)	374.15–393.15	25–690	0
	Koch et al. (1949)	291.45–295.05	0.14–0.21	0
	Morrison and Billett (1952)	286.45–347.85	1	0
	Rosenthal (1954)	293.15	1	0
	Dodds et al. (1956)	273.15–393.15	0.1–700	0
	Houghton et al. (1957)	273.15–373.15	1–36	0
	Shchennikova et al. (1957)	293.15–348.15	1	0
	Ellis (1959)	387.15–621.15	5–160	0
	Garner et al. (1959)	303.15	5–20	0
	Malinin (1959)	473.15–603.15	100–480	0
	Bartels and Wrbitzky (1960)	288.15–311.15	1	0
	Novak et al. (1961)	284.65–350.15	0.15–1	0
	Austin et al. (1963)	293.15–311.15	1	0
	Ellis and Golding (1963)	450.15–607.15	15–75	0
	Tödheide and Franck (1963)	323.15–643.15	200–3550	0
	Takenouchi and Kennedy (1964)	383.15–623.15	100–1480	0
	Yeh and Peterson (1964)	298.15–318.15	1	0
	Takenouchi and Kennedy (1965)	423.15–623.15	100–1380	0
	Vilcu and Gainar (1967)	293.15–308.15	25–75	0
	Gerecke (1969)	288.15–333.15	1	0
	Matous et al. (1969)	303.15–353.15	10–40	0
	Onda et al. (1970a)	298.15	1	0
	Power and Stegall (1970)	310.15	1	0
	Stewart and Munjal (1970)	273.15–298.15	10–45	0
	Barton and Hsu (1971)	273.35–313.15	1	0
	Coan and King (1971)	298.15–373.15	15–50	0
	Hayduk and Malik (1971)	298.15	1	0
	Li and Tsui (1971)	273.85–303.15	1	0
	Murray and Riley (1971)	274.19–308.15	1	0
	Malinin and Savelyeva (1972)	298.15–348.15	47	0
	Malinin and Kurovskaya (1975)	298.15–423.15	47	0
	Angus (1976)	216.58–303.1	5–70	0
	Yasunishi and Yoshida (1979)	288.15–308.15	1	0
	Drummond (1981)	303.85–621.65	40–260	0
	Shagiakhmetov and Tarzimanov (1981)	323.15–423.15	100–790	0
	Won et al. (1981)	298.15	1	0
	Zawisza and Malesińska (1981)	323.15–473.15	1.5–55	0
	Burmakina et al. (1982)	298.15	1	0
	Cramer (1982)	306.15–486.25	8–55	0
	Gillespie et al. (1984)	288.71–533.15	7–200	0
	Briones et al. (1987)	323.15	65–170	0
	Nakayama et al. (1987)	298.15	35–110	0
	Postigo and Katz (1987)	288.15–308.15	1	0

Table 1 (*continued*)

System	Reference	Temperature range, K	Pressure range, atm	Salt concentration mol·kg^{-1} H_2O
CO_2–H_2O	DiSouza et al. (1988)	323.15–348.15	100–150	0
	Müller et al. (1988)	373.15–473.15	3–80	0
	Eremina et al. (1989)	298.15–313.15	1	0
	Nighswander et al. (1989)	352.85–471.25	20–100	0
	Oyevaar et al. (1989)	298.15	1	0
	Traub and Stephan (1990)	313.15	40–100	0
	Carroll et al. (1991)	273.15–433.15	0.5–10	0
	Sterner and Bodnar (1991)	494.15–608.15	480–3060	0
	Sako et al. (1991)	348.15–421.4	100–195	0
	Crovetto and Wood (1992)	623.05–642.65	175–220	0
	King et al. (1992)	288.15–313.15	50–240	0
	Mather and Franck (1992)	273.15–546.45	10–3070	0
	Dohrn et al. (1993)	323.15	100–300	0
	Ohgaki et al. (1993)	283.07–289.37	45–50	0
	Yang and Yuan (1993)	278.15–318.15	1	0
	Rumpf et al. (1994)	323.15	10–55	0
	Vazquez et al. (1994a)	298.15	1	0
	Jackson et al. (1995)	323.15–348.15	340	0
	Fenghour et al. (1996)	405–613	55–240	0
	Scharlin (1996)	273.15–433.15	1	0
	Teng et al. (1997)	278.15–293.15	60–290	0
	Zheng et al. (1997)	278.15–338.15	0.5–0.85	0
	Dhima et al. (1999)	344.15	100–990	0
	Fan and Guo (1999)	283.1	46	0
	Wendland et al. (1999)	281.21–304.63	40–75	0
	Bamberger et al. (2000)	323.15–353.15	40–140	0
	Blencoe et al. (2001)	573.15	270–560	0
	Servio and Englezos (2001)	277.05–283.15	20–40	0
	Kiepe et al. (2002)	313.15–393.15	1–90	0
	Bando et al. (2003)	303.15–333.15	100–200	0
	Chapoy et al. (2004)	274.14–351.31	2–90	0
	Li et al. (2004)	332.15	35–200	0
	Valtz et al. (2004)	278.22–318.23	5–80	0
	Koschel et al. (2006)	323.15–373.15	20–200	0
CO_2–$NaCl$–H_2O	Mackenzie (1877)	279.55–295.15	1	1.3–6
	Setchenow (1892)	288.35	1	0.2–6.1
	Kobe and Williams (1935)	298.15	1	1.9–5.7
	Markham and Kobe (1941)	273.35–313.15	1	0.1–4
	Harned and Davis (1943)	273.15–323.15	1	0.2–3
	Rosenthal (1954)	293.15	1	1.6–5.7
	Ellis and Golding (1963)	445.15–603.15	25–90	0.5–2
	Yeh and Peterson (1964)	298.15–318.15	1	0.16
	Takenouchi and Kennedy (1965)	423.15–723.15	100–1380	1.1–4.3
	Gerecke (1969)	288.15–333.15	1	0.5–4.7
	Onda et al. (1970a)	298.15	1	0.5–3.2
	Malinin and Savelyeva (1972)	298.15–348.15	47	0.4–4.9
	Malinin and Kurovskaya (1975)	298.15–423.15	47	1–6.8
	Yasunishi and Yoshida (1979)	288.15–308.15	1	0.5–5.7
	Gehrig (1980)	408.15–573.15	875–2680	1.1
	Drummond (1981)	292.85–673.15	35–390	1–6.5
	Burmakina et al. (1982)	298.15	1	0.001–0.2
	Cramer (1982)	296.75–511.75	8–60	0.5–2
	Nighswander et al. (1989)	353.15–473.65	20–100	0.17
	He and Morse (1993)	273.15–363.15	0.04–1	0.1–6.1
	Rumpf et al. (1994)	313.15–433.15	5–95	4–6
	Vazquez et al. (1994a)	298.15	1	0.7–2.9
	Vazquez et al. (1994b)	293.15–308.15	1	0.7–2.9
	Zheng et al. (1997)	278.15–338.15	0.5–0.85	0.7–3.3
	Kiepe et al. (2002)	313.15–353.15	1–100	0.5–4.3
	Bando et al. (2003)	303.15–333.15	100–200	0.15–0.55
	Koschel et al. (2006)	323.15–373.15	50–200	1–3
CO_2–KCl– H_2O	Mackenzie (1877)	281.15–295.15	1	0.9–3.9
	Setchenow (1892)	288.35	1	0.9–2.8
	Geffcken (1904)	288.15–298.15	1	0.4–1.1
	Findlay and Shen (1912)	298.15	1	0.25–1
	Markham and Kobe (1941)	273.35–313.15	1	0.1–4
	Gerecke (Gerecke, 1969)	288.15–333.15	1	0.5–3.3
	Yasunishi and Yoshida (1979)	298.15–308.15	1	0.4–4.7
	Burmakina et al. (1982)	298.15	1	0.001–0.2
	He and Morse (1993)	273.15–363.15	0.3–1	0.1–5
	Kiepe et al. (2002)	313.15–353.15	1–100	0.5–4
	Kamps et al. (2007)	313.15–433.15	5–90	1.9–4.1
CO_2–$MgCl_2$–H_2O	Kobe and Williams (1935)	298.15	1	4.5
	Yasunishi and Yoshida (1979)	288.15–308.15	1	0.15–4.4
	He and Morse (1993)	273.15–363.15	0.3–1	0.1–5.0

(*continued on next page*)

Table 1 (*continued*)

System	Reference	Temperature range, K	Pressure range, atm	Salt concentration mol·kg^{-1} H_2O
CO_2–$CaCl_2$–H_2O	Mackenzie (1877)	281.15–303.15	1	0.4–1.7
	Setchenow (1892)	288.35	1	0.15–5
	Kobe and Williams (1935)	298.15	1	6
	Prutton and Savage (1945)	348.65–394.15	15–700	1–3.9
	Malinin (1959)	473.15–623.15	100–390	1
	Onda et al. (1970b)	298.15	1	0.2–2.3
	Malinin and Savelyeva (1972)	298.15–348.15	47	0.2–4.4
	Malinin and Kurovskaya (1975)	373.15–423.15	47	0.9–8.8
	Yasunishi and Yoshida (1979)	298.15–308.15	1	0.2–5.3
	Eremina et al. (1989)	298.15–313.15	1	0.0025–0.025
	He and Morse (1993)	273.15–363.15	0.3–1	0.1–5
CO_2–NaCl– KCl–H_2O	Yasunishi et al. (1979)	298.15	1	0.5–5
CO_2–NaCl–$CaCl_2$–H_2O	Malinin and Savelyeva (1972)	298.15	47	1.4
CO_2–KCl–$CaCl_2$–H_2O	Yasunishi et al. (1979)	298.15	1	0.4–3.9
CO_2–NaCl–KCl–$CaCl_2$–H_2O	Yasunishi et al. (1979)	298.15	1	0.4–3

CO_2 solubility in NaCl, KCl, and $CaCl_2$ solutions, the simplicity of the ion–CO_2 interaction parameters is remarkable and can be expected to contribute to the predictive character of the model across the full range of CO_2 content in the liquid phase, i.e., from the H_2O-rich to the CO_2-rich region. We emphasize that the new experimental data measured in this study have not been used in the determination of parameters. Thus, they provide a stringent test of the predictive capability of the model.

4. Results and discussion

4.1. Measurement of water solubilities in $scCO_2$

Experimental water concentrations in $scCO_2$ in contact with solutions of $CaCl_2$ and NaCl (Table 6) as a function of temperature show the expected trends of increasing water solubility in $scCO_2$ with increasing temperature and decreasing water solubility with increasing electrolyte concentration. Two different solutions of $CaCl_2$ and NaCl were prepared and analyzed. The first set, labeled "Sat" in Table 6, represents solutions that were saturated with the indicated electrolyte solution at 25 °C. The second set, labeled Sat + 3.0 g solid (NaCl) or Sat + 2.16 g solid ($CaCl_2$) were solutions with additional solid phase added to the solution prior to introducing the solution/solid slurry to the experimental system. The presence of additional solid was designed to insure solid/aqueous solution phase equilibrium even as the temperature was increased. The water solubility in $scCO_2$ was then measured for these solutions as a function of temperature. In the case of NaCl the measured water solubilities in $scCO_2$ were nearly the same in both sets 1 and 2 since the solubility of NaCl in water does not increase rapidly with temperature from 40 to 100 °C. However, in the case of $CaCl_2$ the measured water solubility was significantly different between sets 1 and 2 since the solubility of $CaCl_2$ at 25 °C is much lower (~7 m) than at 100 °C (13.6 m, see Table 6). As a result, the measured water solubility in $scCO_2$ in contact with aqueous $CaCl_2$ solutions is much lower in the solutions with additional solid $CaCl_2$ than in the absence of the solid. This comparison also holds across the entire range of electrolyte concentrations examined for both NaCl and $CaCl_2$.

4.2. Modeling phase equilibria in aqueous H_2O–CO_2–Na–Ca–Cl systems

4.2.1. CO_2–H_2O binary

Figs. 1–3 compare the model predictions with experimental data for the CO_2–H_2O binary system. Fig. 1 shows the equilibrium pressure as a function of CO_2 mole fraction in the aqueous phase for five selected isotherms (i.e., 0, 25, 50, 100, and 150 °C). The experimental data in Fig. 1 have been assembled from various sources so that the measured temperatures do not deviate from the temperatures indicated in Fig. 1 by more than 0.2 °C. Since the solubilities of CO_2 in water have been comprehensively reviewed by Diamond and Akinfiev (2003), Duan and Sun (2003) and Spycher et al. (2003), a critical evaluation of the experimental data is outside of the scope of this work. As discussed by Duan and Sun (2003), most CO_2 solubility data in water are consistent within approximately 7% up to 533 K and 2000 atm. Therefore, Fig. 1 combines the CO_2 solubility data from various sources (Table 1). The model reproduces the majority of the data (except for those of Zelvenskii (1937), Dodds et al. (1956), Vilcu and Gainar (1967), Stewart and Munjal (1970), Shagiakhmetov and Tarzimanov (1981) and Kiepe et al. (2002)) within the experimental scattering for pressures up to 3500 atm.

Various data sources for the solubility of H_2O in CO_2 show much greater discrepancies than those for the solubility of CO_2 in H_2O and these discrepancies increase with temperature. Therefore, Figs. 2 and 3 compare the calculated results with individual data sources. Fig. 2a shows the H_2O solubilities in CO_2 for two subcritical isotherms (i.e., 15 °C and 25 °C) and one isotherm that is above the critical point

Table 2
Parameters that determine the thermodynamic properties of individual ionic and neutral species: standard partial molar Gibbs energy of formation, entropy, and parameters of the Helgeson–Kirkham–Flowers equation of state (Helgeson et al. (1974a, 1974b), Helgeson et al. (1976, 1981), Tanger and Helgeson (1988)) for standard partial molar thermodynamic properties ($a_{HKF,1,...4}$,$c_{HKF,1}$, $c_{HKF,2}$, ω).

Species	$\Delta\overline{G}_f^0$ kJ·mol^{-1}	$\overline{S}^0$ J·mol^{-1} K^{-1}	$a_{HKF,1}$	$a_{HKF,2}$	$a_{HKF,3}$	$a_{HKF,4}$	$c_{HKF,1}$	$c_{HKF,2}$	ω
Na^{+a}	−261.881	58.4086	0.1839	−228.5	3.256	−27260	18.18	−29,810	33060
K^{+a}	−282.462	101.044	0.3559	−147.3	5.435	−27120	7.4	−17,910	19270
Mg^{2+a}	−453.960	−138.100	−0.08217	−859.9	8.39	−23900	20.8	−58,920	153720
Ca^{2+a}	−552.790	−56.484	−0.01947	−725.2	5.2966	−24792	9	−25,220	123660
Cl^{-a}	−131.290	56.735	0.4032	480.1	5.563	−28470	−4.4	−57,140	145600
$MgCl_{2(aq)}$[b]	−623.223	2.8920	0.62187	740.58	2.8322	−30851	23.961	32,720	−3800
$CaCl_{2(aq)}$[b]	−794.040	67.7344	0.62187	740.58	2.8322	−30851	23.961	32,720	−3800
$CO_{2(aq)}$[c]	−385.974	117.57	1.50979	0.	−109.419	0.	40.0325	88,004	−2000

[a] Parameters were obtained from Shock and Helgeson (1988) and Shock et al. (1989).
[b] Parameters for the ion pairs were determined in a previous study (Gruszkiewicz et al., 2007) based on multiproperty regressions for aqueous salt solutions.
[c] Parameters adjusted in this study.

Table 3
Binary parameters used in the virial interaction term (Eqs. (8)–(9)).

Species i	Species j	$b_{0,ij}$	$b_{1,ij}$	$b_{2,ij}$	$b_{3,ij}$	$b_{4,ij}$	$c_{0,ij}$	$c_{1,ij}$	$c_{2,ij}$	$c_{3,ij}$	$c_{4,ij}$
Na^+	Cl^-	15610.63	7.964204	−357992.9	−0.003643102	−2892.662	−30086.35	−15.00973	699,848.7	0.006820989	5552.343
K^+	Cl^-	15087.68	7.236058	−354195.6	−0.003141513	−2771.596	−26853.29	−12.85712	635,045.6	0.005649944	4927.578
Mg^{2+}	Cl^-	−46.0902	0.036682	−12896	8.29385e−6	0	110.429	−0.240247	11,645.2	0.000319761	0
Ca^{2+}	Cl^-	−95.9932	0.470226	−17370.9	−5.67551e−4	0	−0.694366	−0.421581	43,725.9	0.000791106	0
Na^+	K^+	−93.0411	−0.234488	37002.7	5.62879e−4	0	−64.633	0.881525	−29,428.5	−0.00128594	0
Na^+	Mg^{2+}	−28.8624	0.0351923	8744.27	0	0	0	0	−6373.88	0	0
Na^+	Ca^{2+}	11.2685	−0.0263793	2905.5	0	0	0	0	−6685.21	0	0
K^+	Mg^{2+}	−28.2506	0.0311345	16139.0	0	0	0	0	−13,262.6	0	0
K^+	Ca^{2+}	−43.804	0.0468862	23092.5	0	0	0	0	−18,687.4	0	0
$CaCl_{2(aq)}$	Na^+	−27.3022	0	17433.	0	0	0	0	0	0	0
$CaCl_{2(aq)}$	K^+	−24.2268	0	18665.2	0	0	0	0	0	0	0
$CaCl_{2(aq)}$	H_2O	−9.09197	0	7761.96	0	0	0	0	0	0	0
$MgCl_{2(aq)}$	Na^+	0	0	−11710.7	0	0	0	0	0	0	0
$MgCl_{2(aq)}$	K^+	0	0	−9228.3	0	0	0	0	0	0	0
$CO_{2(aq)}$	H_2O	−10.2134	0.0102376	783.548	0	0	0	0	0	0	0
$CO_{2(aq)}$	Na^+	−10.9006	0	0	0	0	0	0	0	0	0
$CO_{2(aq)}$	K^+	−8.51244	0	0	0	0	0	0	0	0	0
$CO_{2(aq)}$	Mg^{2+}	−21.1002	0	0	0	0	0	0	0	0	0
$CO_{2(aq)}$	Ca^{2+}	−20.4164	0	0	0	0	0	0	0	0	0

of CO_2 (i.e., 40 °C). The 15 °C and 25 °C isotherms show a transition between vapor–liquid and liquid–liquid equilibria at 50 and 63.3 atm, respectively. The calculations are in a generally good agreement with data from three separate literature sources for the 15 °C isotherm and six sources for the 25 °C isotherm. At 40 °C, a transition is observed between the VLE-like region below ca. 100 atm and an LLE-like region above 100 atm. The calculations are in a reasonable agreement with the data of King et al. (1992) and Traub and Stephan (1990).

Fig. 2b shows the results for the 50 °C and 75 °C isotherms. At 50 °C, literature data are available from seven sources. The data of Wiebe and Gaddy (1939), Coan and King (1971), Briones et al. (1987), and Bamberger et al. (2000) are in an excellent agreement with each other in the VLE region and in the region of transition between the VLE-like and LLE-like behavior. The model accurately reproduces these data. However, substantial discrepancies are observed in the LLE-like region, in which Tödheide and Franck (1963) and DiSouza et al. (1988) report meaningfully higher solubilities than Wiebe and Gaddy (1939). At 75 °C, the model is in a very good agreement with the data of Wiebe and Gaddy (1939) (except for one point at 25 atm) and in a slightly worse but still good agreement with those of DiSouza et al. (1988) and Gillespie et al.(1984). The solubilities of Sako et al. (1991) are substantially lower.

Fig. 3a shows the results for 100 °C and 110 °C. In this temperature region, there is a very large disagreement between the data of Tödheide and Franck (1963) and Takenouchi and Kennedy (1964) in the high-pressure (or LLE-like) region. The possible reasons for the discrepancies between these two data sources have been analyzed by Mather and Franck (1992) and Blencoe et al. (2001) and this topic is beyond the scope of this work. The model is in a very good agreement with the data of Tödheide and Franck (1963) and, consequently, it does not agree with those of Takenouchi and Kennedy (1964). In the lower-pressure (or VLE-like) region, the data of Coan and King (1971) and Müller et al. (1988) are consistent with each other whereas the data of Drummond (1981) are shifted towards lower solubilities. The model is in agreement with the data of Coan and King (1971) and Müller et al. (1988). Fig. 3b compares the calculations with experimental data at 120 °C and 150 °C. The discrepancies between the high-pressure data of Tödheide and Franck (1963) and Takenouchi and Kennedy (1964) persist at 150 °C. At this temperature, the model calculations lie between these two data sets although they are closer to the data of Tödheide and Franck (1963). In the VLE-like region, which extends up to about 200 atm, the data of Gillespie et al.(1984), Müller et al. (1988), and Drummond (1981) are in a good agreement with each other and are accurately represented by the model.

The data in Figs. 2 and 3 also present a comparison of the new measurements made as part of this study for salt-free systems (cf. the solid diamonds in Figs. 2a, b and 3a) with both the literature data and the model calculations. On an overall basis, the new experimental measurements are consistent with the earlier data as well as the model calculations.

Table 4
Pure-component parameters used for modeling gas and solid-phase properties.

Species	ΔG_f^0 kJ·mol^{-1}	S^0 J·mol^{-1} K^{-1}	$Cp = a + bT + \frac{c}{T^2} + dT^2 + eT^3$				
			a	b	c	d	e
CO_2(g)[a,b]	−394.36	213.74	26.2022	0.051162	−169,772	−2.9058e−5	6.20044e−9
Mg_2SiO_4(s)[c]	−2056.70	95.186	149.829	0.027363	−3,564,770	0	0
$MgCO_3{\cdot}3H_2O$(s)[c]	−1723.95	195.644	237.693	0	0	0	0
SiO_2(s, am) [b,c]	−850.54	49.535	74.7479	−0.0075065	−3,118,370	5.71603e−6	0

Species	T_c[d] K	P_c[d] atm	ω[d]	$\alpha(T)$[e]
CO_2(g)	304.12	72.776	0.231	$[1+(0.480+1.574\omega-0.176\omega^2)(1-T_R^{0.5})]^2$
H_2O(g)	647.14	217.755	0.348	$[1+1.318711(1-T_R^{0.5})+2.304407(1-T_R^{0.5})^2]^2$

[a] Wagman et al. (1982).
[b] Gurvich et al. (1990).
[c] Robie and Hemingway (1995).
[d] TRC (1989).
[e] See Eq. (20); expressed in terms of reduced temperature, i.e., $T_R = T/T_c$.

Table 5
Binary parameters used in the short−range interaction term (Eq. (14)) and in the mixing rule for the SRK equation of state (Eq. (22)).

Species i	Species j	$a_{ij}^{(0)}$	$a_{ij}^{(1)}$	$a_{ij}^{(P0)}$	$a_{ij}^{(P1)}$	$k_{ij}^{(0)}$	$k_{ij}^{(1)}$
$CO_{2(aq)}$	H_2O	−3387.02	−0.570569	−0.0085503	−0.000666502	0.195736	47.0126
H_2O	$CO_{2(aq)}$	6809.06	−28.4899	−0.852074	0.00250429	n/a	n/a

4.2.2. CO_2–H_2O–salt ternaries

Figs. 4–10 show representative results of calculating CO_2 solubilities in aqueous chloride salt solutions. Experimental data for such systems (cf. Table 1) encompass numerous measurements of salting out of the gas at near-ambient pressures and moderate temperatures and several sources of data at conditions that coincide or overlap with those of CO_2 sequestration (Prutton and Savage (1945), Malinin and Savelyeva (1972), Malinin and Kurovskaya (1975), Drummond (1981), Cramer (1982), Nighswander et al. (1989), Rumpf et al. (1994), Kamps et al. (2007), Bando et al. (2003), Koschel et al. (2006), Kamps et al. (2007)). Also, measurements at substantially higher temperatures and pressures are available (Malinin (1959), Ellis and Golding (1963), Takenouchi and Kennedy (1965), Gehrig (1980)) and have been used in the determination of model parameters.

Fig. 4 shows the solubility in molality units of CO_2 in aqueous NaCl solutions as a function of salt molality at 1 atm CO_2 and temperatures ranging from 0 °C to 50 °C. Fig. 5 illustrates the CO_2 solubility in the same system at a pressure of 47.33 atm and temperatures ranging from 25 °C to 150 °C. At all temperatures, the solubility decreases with NaCl concentration following a classical salting-out pattern with a slow attenuation of the slope of the solubility vs. salt concentration curve as the concentration of NaCl increases. Fig. 6 shows the temperature dependence of CO_2 solubility over a wide range of temperatures (0 to 300 °C) and NaCl molalities (0 to 6 molal). It should be noted that Fig. 6 does not represent solubility isobars because the data of Drummond (1981) were obtained at pressures that gradually increase with temperature. Thus, the lines in Fig. 6 only link the calculated results at pressures that correspond to the experimental data at each temperature and do not constitute a thermodynamic projection. As shown in Fig. 6, the experimental data (Drummond, 1981) show more scattering than those in Figs. 4–5. Nevertheless the calculated temperature trends are consistent with the data. Fig. 7 shows the pressure dependence of CO_2 solubilities in NaCl solutions at temperatures ranging from 40 °C to 160 °C and salt molalities from 0.52 m to 6 m. For clarity, this figure is subdivided into two diagrams (7a and 7b) to avoid the overlapping of solubility curves at various conditions. In the pressure range from 1 to 100 atm, the phase behavior is in the VLE-like range and, therefore, the CO_2 solubility increases with pressure with a relatively constant slope. The slope decreases as the pressure approaches ~100 atm, reflecting a transition to an LLE-like region. As shown in Figs. 4–7, the model accurately reproduces the dependence of CO_2 solubility on temperature, pressure, and NaCl concentration in wide ranges of these variables, which encompass and go substantially beyond the conditions of CO_2 sequestration.

The behavior of CO_2 in KCl solutions is similar to that in NaCl solutions. This is illustrated in Fig. 8, which compares the calculations with experimental data for temperatures up to 160 °C, pressures up to 100 atm and KCl concentrations up to 4 molal.

Table 6
Water solubility of saturated NaCl and $CaCl_2$ solutions in $scCO_2$ at 90 atm and different temperatures determined by NIR absorption spectroscopic measurements.

Temp. °C	NaCl molality	$CaCl_2$ molality	H_2O Mol%
40	0	0	0.32
40	Sat. NaCl	0	0.22
40	Sat NaCl + 3.0 g solid	0	0.25
40	0	Sat. $CaCl_2$	0.16
40	0	Sat $CaCl_2$ + 2.16 g solid	0.05
50	0	0	0.49
50	2	0	0.48
50	4	0	0.47
50	6	0	0.38
50	Sat. NaCl	0	0.40
50	Sat NaCl + 3.0 g solid	0	0.42
50	0	0.85	0.44
50	0	2.94	0.31
50	0	5.62	0.20
50	0	Sat. $CaCl_2$	0.17
50	0	Sat $CaCl_2$ + 2.16 g solid	0.11
75	0	0	0.85
75	Sat. NaCl	0	0.88
75	Sat NaCl + 3.0 g solid	0	0.89
75	0	Sat. $CaCl_2$	0.62
75	0	Sat $CaCl_2$ + 2.16 g solid	0.20
100	0	0	1.61
100	Sat. NaCl	0	1.68
100	Sat NaCl + 3.0 g solid	0	1.60
100	0	Sat. $CaCl_2$	1.12
100	0	Sat $CaCl_2$ + 2.16 g solid	0.46

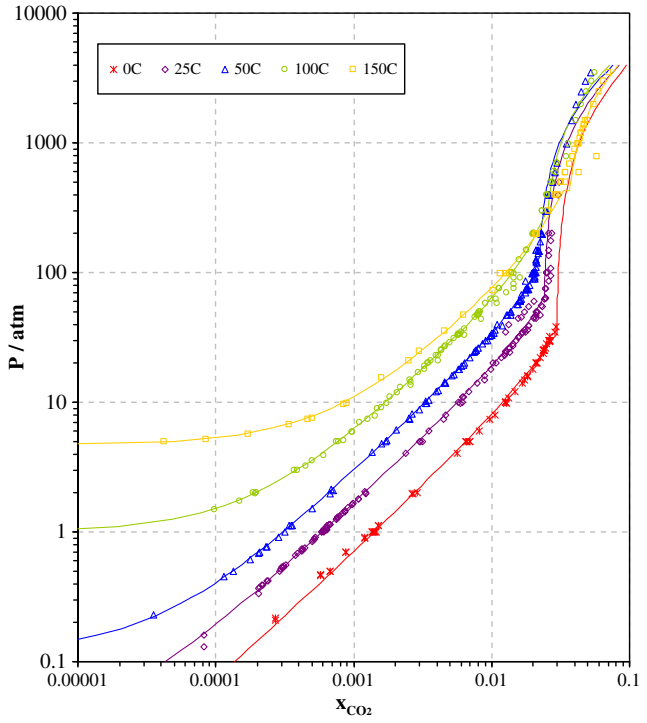

Fig. 1. Calculated and experimental solubility of CO_2 in H_2O at 0, 25, 50, 100, and 150 °C. The experimental data are from Prytz and Holst (1895), Findlay and Creighton (1910), Findlay and Shen (1912), Findlay and Williams (1913), Findlay and Howell (1915), Morgan and Pyne (1930), Morgan and Maass (1931), Kobe and Williams (1935), Shedlovsky and MacInnes (1935), Zelvenskii (1937), Wiebe and Gaddy (1939, 1940, 1941), Markham and Kobe (1941), Harned and Davis (1943), Dodds et al. (1956), Houghton et al. (1957), Novak et al. (1961), Tödheide and Franck (1963), Takenouchi and Kennedy (1964, 1965), Yeh and Peterson (1964), Vilcu and Gainar (1967), Matous et al. (1969), Stewart and Munjal (1970), Hayduk and Malik (1971), Murray and Riley (1971), Malinin and Savelyeva (1972), Malinin and Kurovskaya (1975), Drummond (1981), Shagiakhmetov and Tarzimanov (1981), Won et al. (1981), Zawisza and Malesińska (1981), Gillespie et al. (1984), Briones et al. (1987), Nakayama et al. (1987), Postigo and Katz (1987), DiSouza et al. (1988), Müller et al. (1988), Oyevaar et al. (1989), Carroll et al. (1991), King et al. (1992), Mather and Franck (1992), Dohrn et al. (1993), Rumpf et al. (1994), Bamberger et al. (2000), Kiepe et al. (2002), Bando et al. (2003), Chapoy et al. (2004), Valtz et al. (2004).

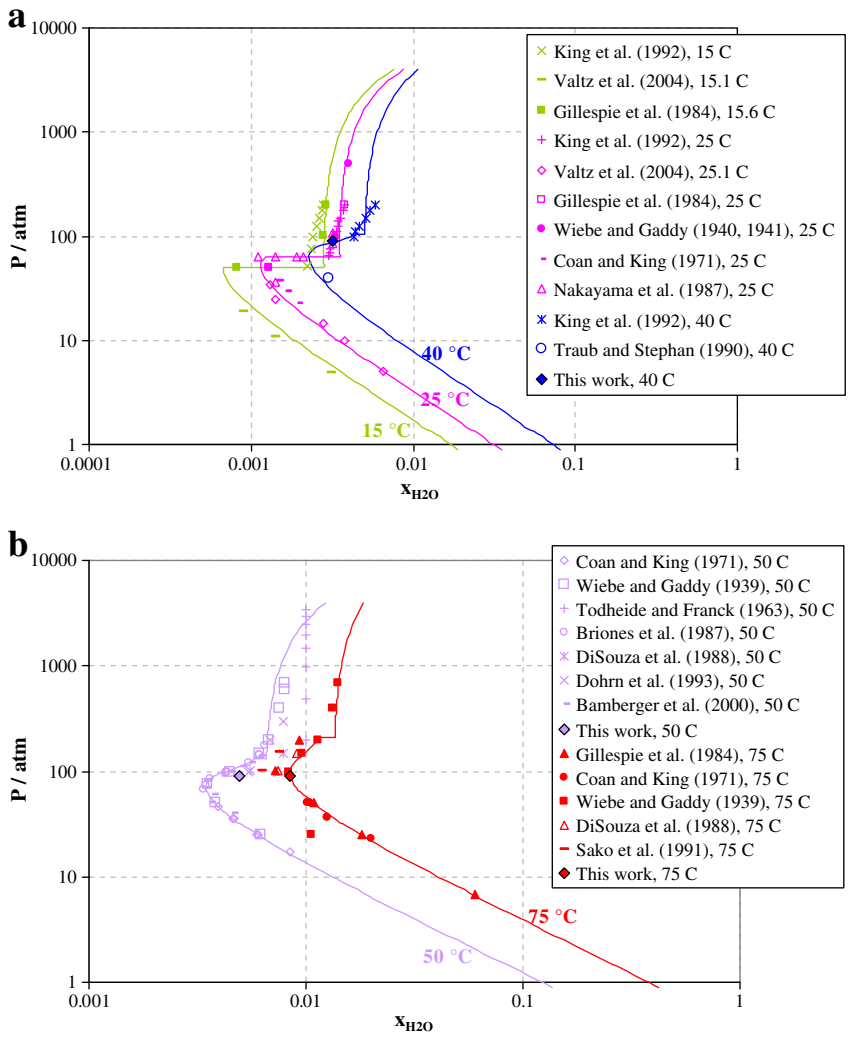

Fig. 2. Calculated and experimental solubility of H_2O in CO_2 at (a) 15, 25, and 40 °C and (b) 50 and 75 °C.

Measurements of CO_2 solubilities in $CaCl_2$ solutions are available over wider ranges of salt concentration than in NaCl and KCl solutions. Fig. 9 shows the calculated and experimental CO_2 solubilities at 47.33 atm CO_2 and temperatures from 25 °C to 150 °C. Thus, Fig. 9 is analogous to Fig. 5 for NaCl solutions. The decrease in CO_2 solubility as a function of $CaCl_2$ concentration is substantially stronger than in NaCl solutions when the CO_2 solubility is plotted as a function of salt molality. Fig. 10 illustrates the effect of pressure on the solubility of CO_2 in $CaCl_2$ solutions at temperatures ranging from 75 °C to 120 °C and pressures up to 1000 atm. For clarity, Fig. 10 is subdivided into two diagrams for $CaCl_2$ concentrations of 1, 3.9, and 2.3 molal. As shown in Fig. 10, the CO_2 solubility transitions from a VLE-like region with a higher slope of CO_2 molality vs. pressure to an LLE-like region with a lower slope. The model accurately represents the solubilities including the change in slope.

As illustrated by Figs. 4–10, the model provides an accurate representation of experimental data for water-rich phases in CO_2–water–chloride salt systems. With the parameters determined on the basis of such data, it is then applied to predict the properties of CO_2-rich phases.

4.2.3. Prediction of water solubility in CO_2-rich phases

Figs. 11 and 12 compare the model predictions with the new experimental data for water solubility in CO_2-rich phases. These figures show the solubility of H_2O in the CO_2-rich phase as a function of salt molality in the coexisting H_2O-rich phase. Fig. 11 presents the results for the CO_2–H_2O–NaCl system. On an overall basis, the effect of NaCl concentration on the water solubility is small. As we will discuss below, this results from the relatively small change in water activity that occurs in NaCl solutions even at high concentration. At 40 °C, the model predictions match the data almost exactly. At 50 °C, the calculated solubilities are offset by a constant amount relative to the data. This offset is due to the small difference between the model calculations and the new data for salt-free systems, as illustrated in Fig. 2b. This offset remains constant as a function of NaCl molality, thus indicating that the predicted effect of NaCl is the same as that indicated by the data. At 75 °C, the model is in an exact agreement with the data in a NaCl-free system and somewhat underestimates the solubility in the presence of concentrated NaCl solutions. At 100 °C, the model predicts a slightly higher H_2O solubility in a salt-free system and is in a good agreement with the data in the presence of concentrated NaCl. Thus, in view of the nature of the deviations, it can be concluded that the model predictions are consistent with the new measurements.

In contrast to NaCl, $CaCl_2$ has a substantial effect on the H_2O solubility in CO_2 owing to the much lower water activity in $CaCl_2$ solutions. As shown in Fig. 12, the H_2O solubility significantly decreases with $CaCl_2$ concentration. At 40 °C and 50 °C, the model is in a good agreement with the data except for one solubility point for 11.7 molal $CaCl_2$. At 75 °C, the model underpredicts the data for 7.2 molal $CaCl_2$ whereas the agreement is reasonably good for 12.4 molal $CaCl_2$. At 100 °C, the model slightly underpredicts the solubilities for 7.2 and 13.6 molal

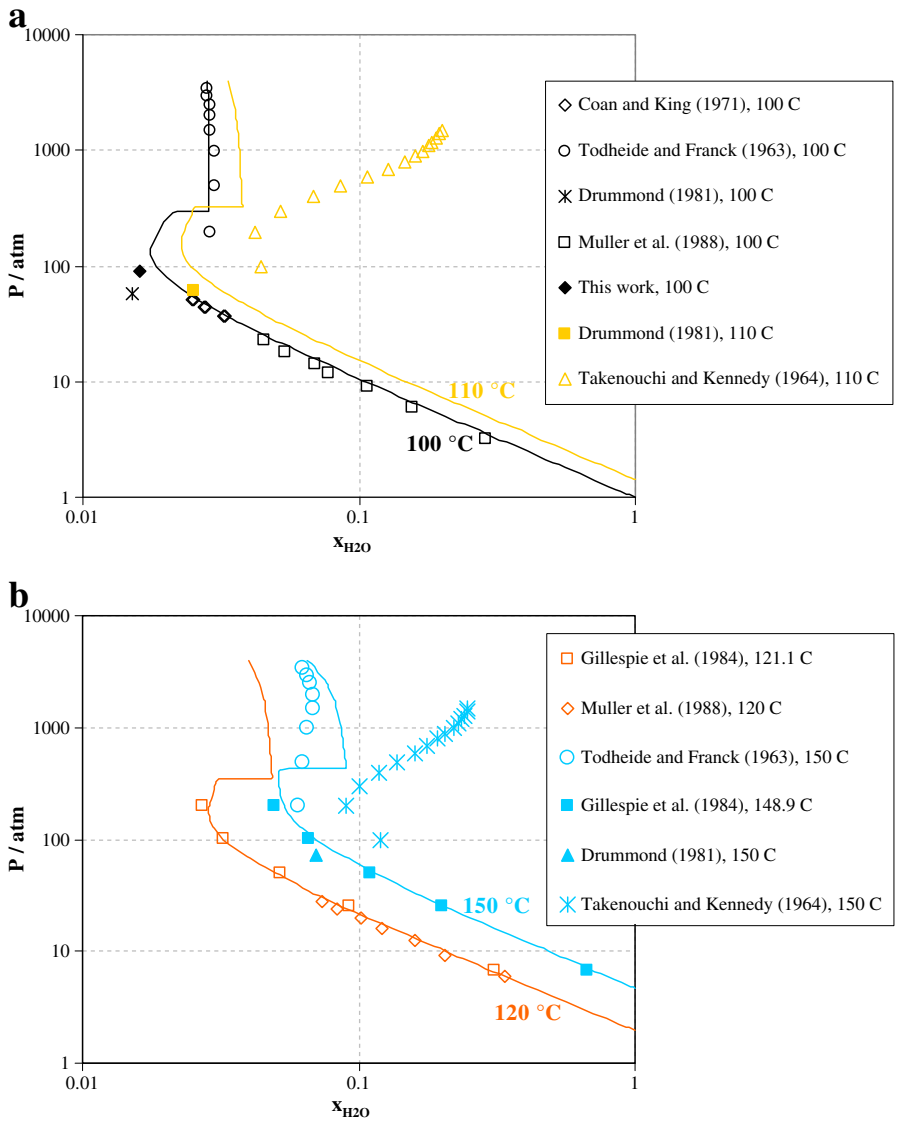

Fig. 3. Calculated and experimental solubility of H_2O in CO_2 at (a) 100 and 110 °C and (b) 120 and 150 °C.

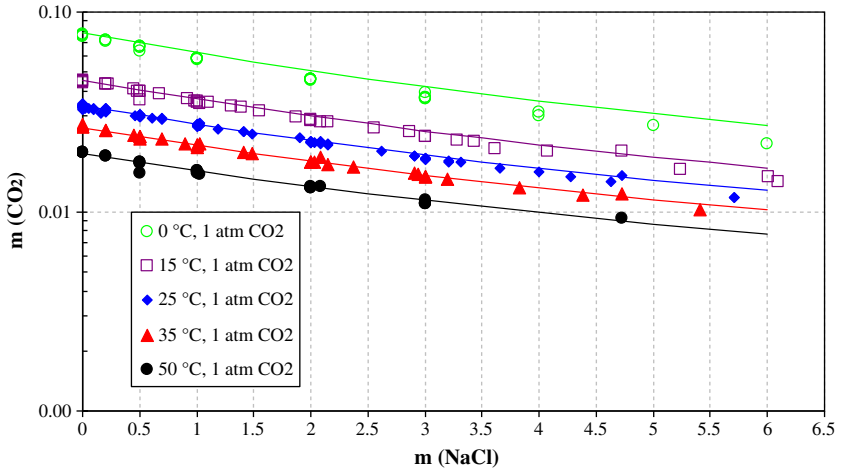

Fig. 4. Calculated and experimental molality of CO_2 in aqueous NaCl solutions at a CO_2 partial pressure of 1 atm as a function of NaCl molality. The experimental data are from Burmakina et al. (1982), Gerecke (1969), Harned and Davis (1943), He and Morse (1993), Kobe and Williams (1935), Mackenzie (1877), Markham and Kobe (1941), Onda et al. (1970a, 1970b), Setchenow (1892), Vazquez et al. (1994a, 1994b), Yasunishi and Yoshida (1979), and Yeh and Peterson (1964).

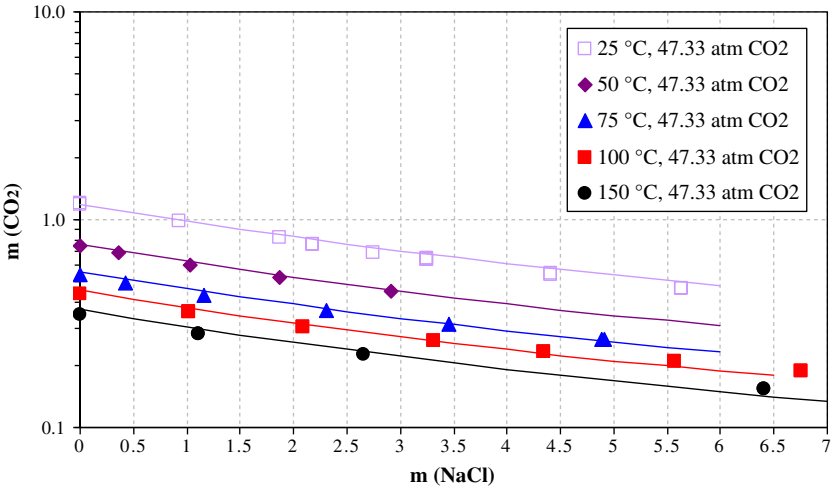

Fig. 5. Calculated and experimental molality of CO_2 in aqueous NaCl solutions at a CO_2 partial pressure of 47.33 atm as a function of NaCl molality. The experimental data are from Malinin and Savelyeva (1972) at temperatures up to 75 °C and from Malinin and Kurovskaya (1975) at 100 °C and 150 °C.

$CaCl_2$. Considering the nature of deviations between the model calculations and the data in Fig. 12, it can be concluded that the model is in a reasonable agreement with the data.

It is also of interest to discuss the precise reasons for the differences in water solubility between the NaCl and $CaCl_2$ solutions observed in the CO_2-rich phase. In this regard, Table 7 presents a comparison between the calculated water concentrations in the CO_2-rich phase with the aqueous water activities and the water fugacity coefficients in the CO_2-rich phase. As expected, the water concentrations in the CO_2-rich phase follow the expected trend of decreasing concentration in the CO_2-rich phase with lower water activity in the aqueous phase. However, the exact relationship between the aqueous water activity and the water concentration in the CO_2-rich phase is a function of temperature. This results in changes in water fugacity coefficients in the CO_2-rich phase with temperature (see Table 7). However, at a given temperature and pressure, the water fugacity coefficients in the CO_2-rich phase do not vary much with aqueous salt concentration since the water activity in the CO_2-rich phase is primarily determined by the bulk CO_2-water interactions. It should be noted that the calculated water activities in the aqueous phase are not significantly impacted by the dissolved CO_2 concentration, even though significant CO_2 does dissolve into the aqueous phase. Thus, the prediction of salt effects on H_2O solubility in CO_2 depends to a large extent on the properties of aqueous solutions regardless of the presence or absence of CO_2. This indicates that reasonable predictions can be made for systems containing a large variety of salts for which aqueous phase properties are known.

5. Application to the formation of hydrated minerals in low water content $scCO_2$ systems

As mentioned in the Introduction, recent experimental research has highlighted the importance of mineral reactivity in low water content CO_2-rich systems. Hence, one of the primary objectives of this study is to develop the capability to predict mineral transformations in the CO_2-rich phase at low water content. In that regard, it is illustrative to demonstrate how the model can be applied to predict mineral transformations as a function of water content in the CO_2-rich phase. To illustrate this effect we have chosen to model the conversion of the mineral forsterite (Mg_2SiO_4) to hydrated magnesium carbonate compounds (e.g. nesquehonite ($MgCO_3 \cdot 3H_2O$). Such transformations have

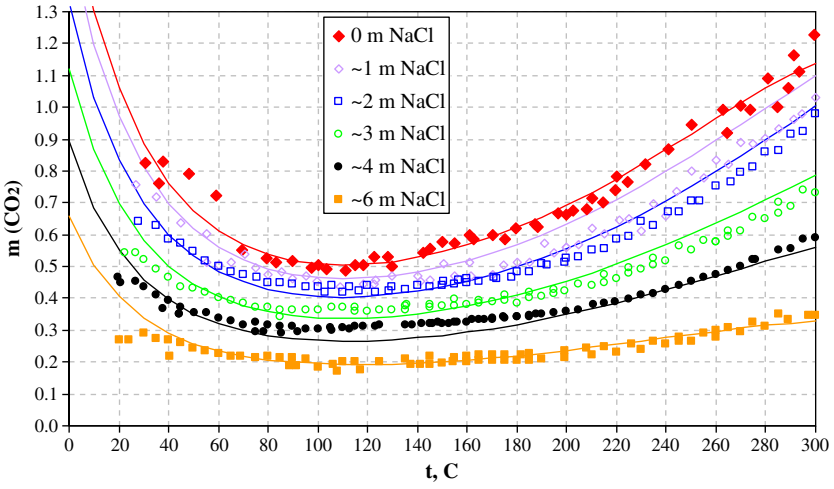

Fig. 6. Calculated and experimental molality of CO_2 in aqueous NaCl solutions as a function of temperature for various NaCl concentrations. The experimental data are from Drummond (1981) and were obtained at pressures that gradually increase with temperature. The total pressure ranges from 38.59 to 179.98 atm at 0 m NaCl, from 41.65 to 198.35 atm at 1 m, from 42.21 to 209.92 atm at 2 m, from 39.96 to 207.33 atm at 3 m, from 34.85 to 189.63 atm at 4 m and from 34.03 to 169.49 atm at 6 m NaCl.

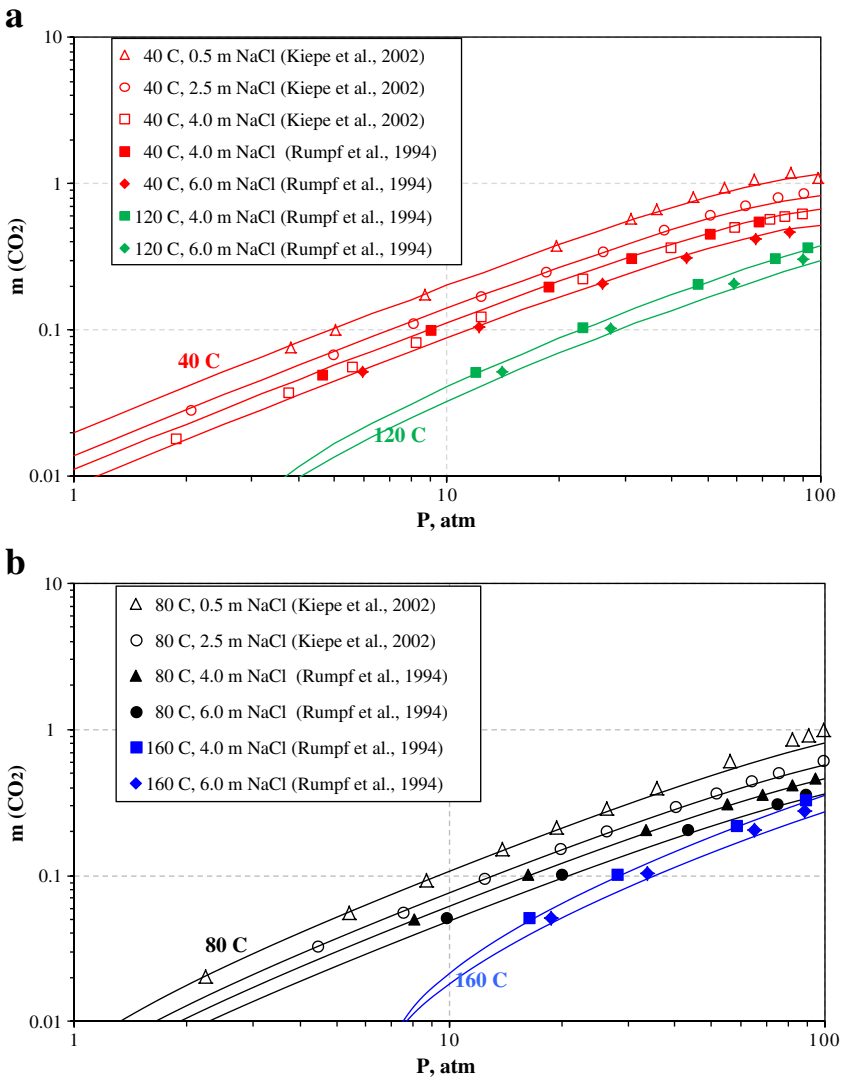

Fig. 7. Calculated and experimental molality of CO_2 in aqueous NaCl solutions at (a) 40 °C and 120 °C and (b) 80 °C and 160 °C as a function of pressure in a moderate pressure range. The experimental data are from Kiepe et al. (2002) and Rumpf et al.(1994).

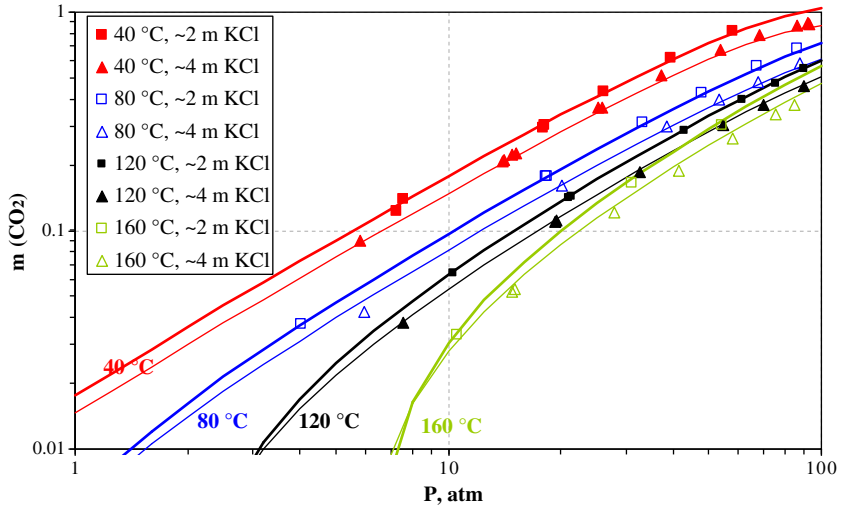

Fig. 8. Calculated and experimental molality of CO_2 in KCl solutions as a function of pressure in a moderate pressure range at temperatures ranging from 40 °C to 160 °C. The experimental data are from Kamps et al. (2007). The thick and thin lines denote the calculations for 2 m and 4 m solutions, respectively.

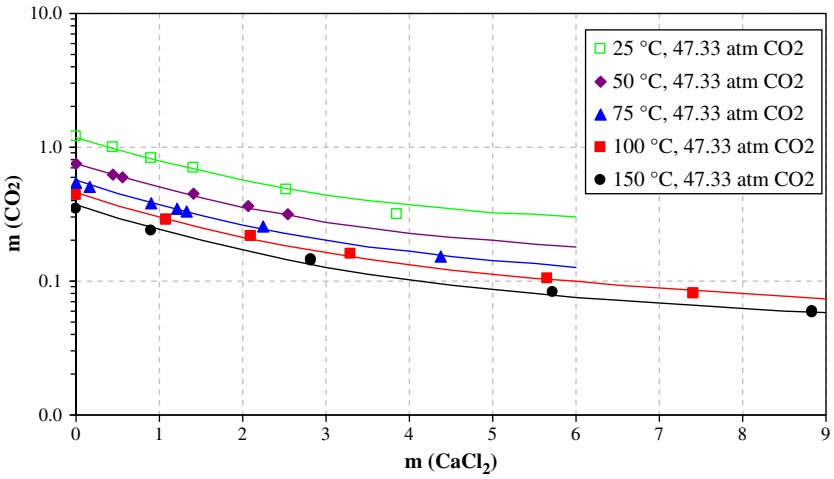

Fig. 9. Calculated and experimental molality of CO_2 in aqueous $CaCl_2$ solutions at a CO_2 partial pressure of 47.33 atm as a function of $CaCl_2$ molality. The experimental data are from Malinin and Savelyeva (1972) at 25 °C, 50 °C, and 75 °C and from Malinin and Kurovskaya (1975) at 100 °C and 150 °C.

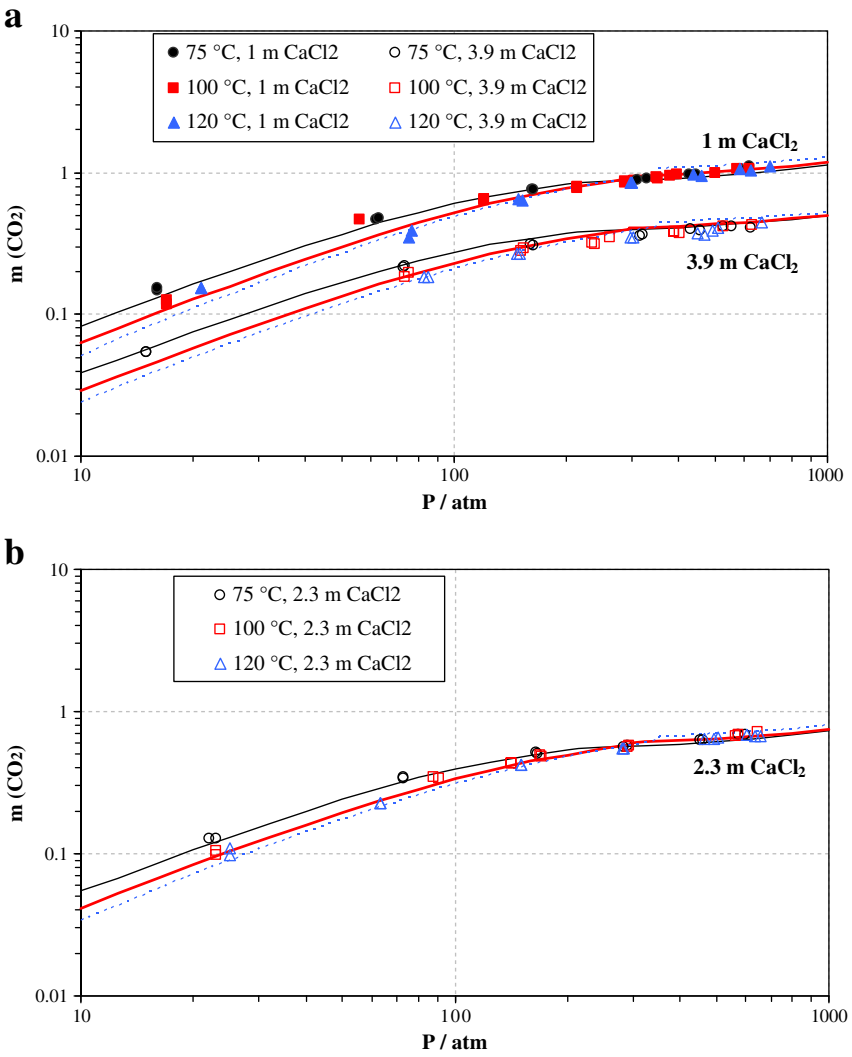

Fig. 10. Calculated and experimental molality of CO_2 in aqueous $CaCl_2$ solutions as a function of pressure at the temperatures of 75, 100, and 120 °C and $CaCl_2$ concentrations of (a) 1 and 3.9 molal and (b) 2.3 molal. The experimental data are from Prutton and Savage (1945). The solubility isotherms at 75, 100, and 120 °C are denoted by the thin solid, thick solid, and dotted lines, respectively.

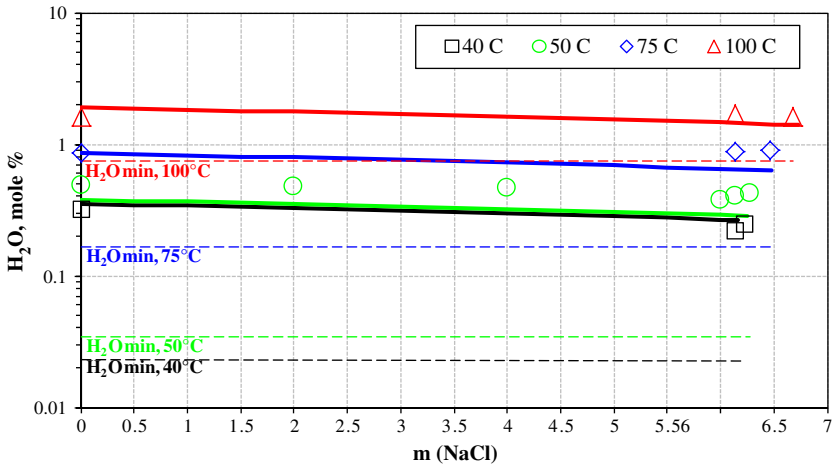

Fig. 11. Comparison of model predictions with new experimental results obtained in this study for the solubility of water (in mole% units) in the CO_2-rich phase in the NaCl–CO_2–H_2O system as a function of NaCl molality in the H_2O-rich phase at 90 atm. The symbols show the experimental data (Table 6). The solid lines show the H_2O solubilities obtained from the model. The near-horizontal dashed lines denote the minimum H_2O mole percent that is required for the transformation of forsterite into nesquehonite.

previously been demonstrated to occur in low water content $scCO_2$ systems (Loring et al., 2011; Felmy et al., 2012). The overall transformation reaction in $scCO_2$ is

$$Mg_2SiO_4 + 2CO_2 + 6H_2O \rightarrow 2MgCO_3 \cdot 3H_2O + SiO_2(am) \quad (23)$$

In the above reaction the water is dissolved in $scCO_2$. Hence, in order to predict the transformation of forsterite to nesquehonite, an accurate model is required for the water fugacity in $scCO_2$ as well as the other phases in the system. Table 8 shows the results of our model calculations of the water concentration in $scCO_2$ required to achieve phase equilibrium between forsterite and nesquehonite at the solution compositions measured in this study. The procedure for making such calculations is outlined in the Appendix A. Also, Table 8 shows the calculated concentrations of H_2O in the $scCO_2$ phase, which correspond to the experimental measurements detailed in Table 6. The results show that at lower temperatures forsterite should transform to nesquehonite even at relatively low water saturations in $scCO_2$. However, as the temperature increases, the water concentration required for nesquehonite to form also increases. In fact, this effect becomes so large that at temperatures greater than 75 °C nesquehonite should not form at all from forsterite in H_2O-saturated $scCO_2$ that is in contact with highly concentrated $CaCl_2$ solutions since the required water saturation is greater than 100%.

6. Conclusions

Determining the chemical potential of variable concentrations of H_2O in supercritical CO_2-rich phases has been approached using a combination of experimental measurements and thermodynamic modeling. New measurements provide data on the solubility of water in the carbon dioxide-rich phase of ternary mixtures of CO_2, H_2O and NaCl or $CaCl_2$. Thus, the new measurements fill a major gap in the experimental database for CO_2–water–salt systems, for which data have been previously available only for the H_2O-rich phase. At the same time, a comprehensive thermodynamic model has been established for predicting the properties of CO_2–H_2O–chloride salt systems in both the H_2O-rich and CO_2-rich phases. This model takes advantage of the large existing database for both phases in the CO_2–H_2O binary and the H_2O-rich phase in the CO_2–H_2O–NaCl/KCl/$CaCl_2$/$MgCl_2$ ternary and multicompontent systems. The model, based on the previously developed MSE framework for mixtures of electrolytes and nonelectrolytes over wide ranges of concentrations and temperatures, represents the properties of these systems essentially within the experimental scattering. Furthermore, the model predicts

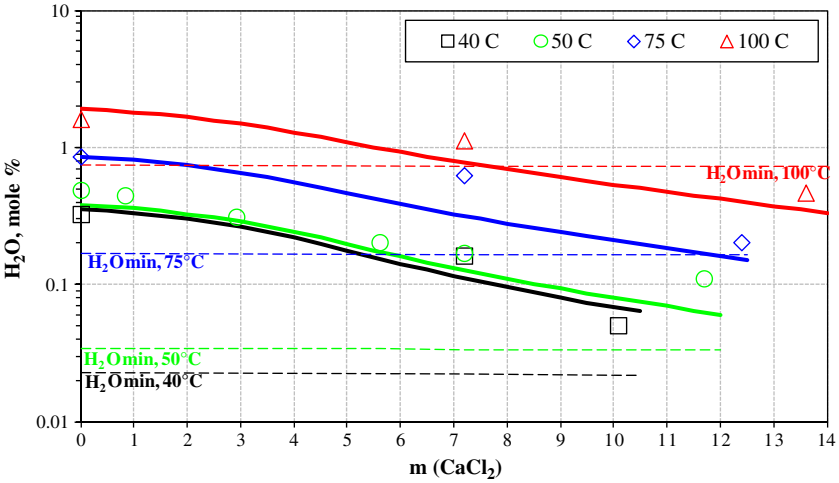

Fig. 12. Comparison of model predictions with new experimental results obtained in this study for the solubility of water (in mole% units) in the CO_2-rich phase in the $CaCl_2$–CO_2–H_2O system as a function of $CaCl_2$ molality in the H_2O-rich phase at 90 atm. The symbols show the experimental data (Table 6). The solid lines show the H_2O solubilities obtained from the model. The near-horizontal dashed lines denote the minimum H_2O mole percent that is required for the transformation of forsterite into nesquehonite (cf. Table 8).

Table 7
Calculated water concentrations, activities and activity/fugacity coefficients in the CO_2-rich phase as a function of temperature and salt concentrations.

Temp. °C	NaCl molality	$CaCl_2$ molality	CO_2 molality	Aqueous H_2O activity	H_2O mole fraction in CO_2-rich phase	H_2O fugacity coefficient in CO_2-rich phase	CO_2 fugacity coefficient in CO_2-rich phase	H_2O Activity in absence of CO_2
40	0	0	1.2357	0.9776	0.003538	0.2373	0.6275	1
40	6.14	0	0.4991	0.7437	0.002655	0.2408	0.6279	0.7548
40	6.22	0	0.4950	0.7403	0.002645	0.2405	0.6277	0.7512
40	0	7.2	0.2740	0.3155	0.001103	0.2461	0.6281	0.3182
40	0	10.1	0.1946	0.1941	0.000673	0.2483	0.6285	0.1957
50	0	0	1.1046	0.9802	0.003789	0.3700	0.6744	1
50	2	0	0.7722	0.9133	0.003526	0.3706	0.6744	0.9304
50	4	0	0.5739	0.8359	0.003221	0.3713	0.6744	0.8492
50	6	0	0.4517	0.7516	0.002889	0.3725	0.6747	0.7617
50	6.14	0	0.4451	0.7456	0.002866	0.3724	0.6746	0.7555
50	6.27	0	0.4392	0.7401	0.002845	0.3723	0.6746	0.7497
50	0	0.85	0.7768	0.9395	0.003628	0.3706	0.6745	0.9572
50	0	2.94	0.4095	0.7523	0.002890	0.3730	0.6749	0.7616
50	0	5.62	0.2739	0.4540	0.001732	0.3760	0.6753	0.4574
50	0	7.2	0.2362	0.3310	0.001259	0.3771	0.6754	0.3335
50	0	11.7	0.1420	0.1654	0.000627	0.3787	0.6755	0.1663
75	0	0	0.8683	0.9847	0.008499	0.5122	0.7545	1
75	6.14	0	0.3495	0.7513	0.006452	0.5147	0.7544	0.7590
75	6.46	0	0.3383	0.7378	0.006334	0.5148	0.7543	0.7452
75	0	7.2	0.1730	0.3699	0.003151	0.5201	0.7549	0.3719
75	0	12.4	0.1035	0.1809	0.001536	0.5240	0.7558	0.1816
100	0	0	0.7459	0.9869	0.018909	0.5961	0.8111	1
100	6.14	0	0.2983	0.7580	0.014409	0.6004	0.8109	0.7647
100	6.68	0	0.2821	0.7361	0.013986	0.6011	0.8110	0.7422
100	0	7.2	0.1396	0.4085	0.007694	0.6092	0.8117	0.4103
100	0	13.6	0.0812	0.1859	0.003485	0.6157	0.8128	0.1864

the solubility of H_2O in CO_2-rich phases in agreement with the new measurements for the CO_2–H_2O–NaCl and CO_2–H_2O–$CaCl_2$ systems. Considering the fact that, in the foreseeable future, experimental data for CO_2-rich phases in equilibrium with salt-containing H_2O-rich phases are likely to be scarce, the model can be used with confidence to predict the effect of various salts on the concentration and activity of H_2O in CO_2-rich phases. Since H_2O activity in CO_2-rich phases plays a key role in mineral reactivity in CO_2 sequestration environments and the MSE model combines phase and chemical equilibria in a uniform formalism, the model is expected to provide a useful tool for predicting mineral transformations in supercritical CO_2.

Table 8
The water mole fraction in the CO_2-rich phase required for equilibrium between forsterite and nesquehonite (rxn 23) as a function of temperature and aqueous salt concentration at 90 atm $scCO_2$ pressure. Details on the calculations of water concentrations are given in the Appendix A.

Temp. °C	NaCl molality	$CaCl_2$ molality	H_2O mole fraction at saturation	H_2O mole fraction required for reaction	% water saturation required for reaction
40	0	0	0.003538	0.0002288	6
40	6.14	0	0.002655	0.0002257	8
40	6.22	0	0.002645	0.0002258	9
40	0	7.2	0.001103	0.0002208	20
40	0	10.1	0.000673	0.0002191	33
50	0	0	0.003789	0.0003419	9
50	2	0	0.003526	0.0003413	10
50	4	0	0.003221	0.0003407	11
50	6	0	0.002889	0.0003399	12
50	6.14	0	0.002866	0.0003399	12
50	6.27	0	0.002845	0.0003399	12
50	0	0.85	0.003628	0.0003414	9
50	0	2.94	0.002890	0.0003397	12
50	0	5.62	0.001732	0.0003373	19
50	0	7.2	0.001259	0.0003364	27
50	0	11.7	0.000627	0.0003351	53
75	0	0	0.008499	0.001669	20
75	6.14	0	0.006452	0.001659	26
75	6.46	0	0.006334	0.001658	26
75	0	7.2	0.003151	0.001645	52
75	0	12.4	0.001536	0.001641	102
100	0	0	0.018909	0.007455	39
100	6.14	0	0.014409	0.007384	51
100	6.68	0	0.013986	0.007382	53
100	0	7.2	0.007694	0.007314	95
100	0	13.6	0.003485	0.007286	209

Acknowledgment

This work was supported by the U. S. Department of Energy (DOE), Office of Basic Energy Sciences through a Single Investigator Small Group Research (SISGR) grant at Pacific Northwest National Laboratory (PNNL). The experimental work was performed at EMSL, the Environmental Molecular Sciences Laboratory, a national scientific user facility sponsored by the Department of Energy's DOE Office of Biological and Environmental Research, and located at PNNL. PNNL is operated for DOE by Battelle Memorial Institute under Contract # DE-AC06-76RLO-1830.

Appendix A. A shortcut procedure for calculating the necessary water content for mineral conversion

The equilibrium condition for the mineral conversion reaction (Eq. (23)) can be calculated from the standard thermodynamic relationship

$$\ln K = -\frac{1}{RT}\sum_i \nu_i \Delta G_{fi}^0 = \ln \prod_i f_i^{\nu_i} \tag{A1}$$

When applied to Eq. (23), the equilibrium relationship becomes

$$\ln K = -\frac{1}{RT}\left(2\Delta G_f^0\left(MgCO_3\cdot 3H_2O_{(s)}\right) + \Delta G_f^0\left(SiO_{2(s)}\right) - \Delta G_f^0\left(Mg_2SiO_{4(s)}\right) - 2\Delta G_f^0\left(CO_{2(g)}\right) - 6\Delta G_f^0\left(H_2O_{(g)}\right)\right) \tag{A2}$$

and

$$K = \frac{1}{f_{CO_2}^2 f_{H_2O}^6} = \frac{1}{\left(Px_{CO_2}\phi_{CO_2}\right)^2\left(Px_{H_2O}\phi_{H_2O}\right)^6} \quad \text{(A3)}$$

In Eq. (A2), the standard Gibbs energies of formation for solid $MgCO_3{\cdot}3H_2O$, Mg_2SiO_4 and SiO_2(am) and ideal-gas CO_2 and H_2O are calculated using the thermochemical data that are summarized in Table 4. The fugacity coefficients in Eq. (A3) are obtained from the model described in this study. As shown in Table 7, the fugacity coefficients of CO_2 and H_2O in the CO_2-rich phase are very weak functions of composition at a given temperature and pressure. Therefore, it can be assumed that they remain practically constant within a reasonable range of water contents. Further, it can be assumed that there is no appreciable dissolution of the minerals in the CO_2-rich phase that would affect the fugacity coefficients. With these assumptions, the water mole fraction that is necessary for the transformation of forsterite into nesquehonite can be calculated as

$$x_{H_2O} = \frac{1}{P\phi_{H_2O}} \exp\left[-\frac{1}{6}\left(\ln K + 2\ln f_{CO_2}\right)\right] \quad \text{(A4)}$$

The fugacity coefficients that are necessary to apply Eq. (A4) are listed in Table 7 at the conditions of the experiments reported in this study.

References

Abrams, D.S., Prausnitz, J.M., 1975. Statistical thermodynamics of liquid mixtures–new expressions for excess Gibbs energy of partly or completely miscible systems. AICHE Journal 21, 116–128.

Akinfiev, N.N., Diamond, L.W., 2010. Thermodynamic model of aqueous CO_2-H_2O-NaCl solutions from −22 to 100 C and from 0.1 to 100 MPa. Fluid Phase Equilibria 295, 104–124.

Anderko, A., Malanowski, S., 1992. Modeling Phase Equilibria: Thermodynamic Background and Practical Tools. J. Wiley & Sons, New York, NY.

Anderko, A., Pitzer, K.S., 1993. Equation of state representation of phase equilibria and volumetric properties of the systems NaCl-H_2O above 573 K. Geochimica et Cosmochimica Acta 57, 1657–1680.

Anderko, A., Wang, P., Rafal, M., 2002. Electrolyte solutions: from thermodynamic and transport property models to the simulation of industrial processes. Fluid Phase Equilibria 194, 123–142.

Angus, S., 1976. International Thermodynamic Tables of the Fluid State. Volume 3: Carbon Dioxide. Butterworths.

Austin, W.H., Lacombe, E., Rand, P.W., Chatterjee, M., 1963. Solubility of carbon dioxide in serum from 15 to 38 C. Journal of Applied Physiology 18, 301–304.

Bachu, S., 2002. Sequestration of CO_2 in geological media in response to climate change: road map for site selection using the transform of the geological space into the CO_2 phase space. Energy Conversion and Management 43, 87–102.

Bachu, S., 2008. CO_2 storage in geological media: role, means, status and barriers to deployment. Progress in Energy and Combustion Science 34, 254–273.

Bachu, S., Adams, J.J., 2003. Sequestration of CO_2 in geological media in response to climate change: capacity of deep saline aquifers to sequester CO_2 in solution. Energy Conversion and Management 44, 3151–3175.

Bamberger, A., Sieder, G., Maurer, G., 2000. High-pressure (vapor + liquid) equilibrium in binary mixtures of (carbon dioxide + water or acetic acid) at temperatures from 313 to 353 K. Journal of Supercritical Fluids 17, 97–110.

Bando, S., Takemura, F., Nishio, M., Hihara, E., Akai, M., 2003. Solubility of CO_2 in aqueous solutions of NaCl at (30 to 60) C and (10 to 20) MPa. Journal of Chemical and Engineering Data 48, 576–579.

Barta, L., Bradley, D.J., 1985. Extension of the specific interaction model to include gas solubilities in high-temperature brines. Geochimica et Cosmochimica Acta 49, 195–203.

Bartels, H., Wrbitzky, R., 1960. Bestimmung des CO_2 Absorptionskoeffizienten zwischen 15 und 38 C in Wasser und Plasma. Pflügers Archiv 271, 162–168.

Barton, J.R., Hsu, C.C., 1971. Solubility of cyclopropane in alkyl carboxylic acids. Journal of Chemical and Engineering Data 16, 93–95.

Benson, S.M., Surles, T., 2006. Carbon dioxide capture and storage: an overview with emphasis on capture and storage in deep geological formations. Proceedings of the IEEE 94, 1795–1805.

Blencoe, J.G., Naney, M.T., Anovitz, L.M., 2001. The CO_2–H2O system: III. A new experimental method for determining liquid–vapor equilibria at high subcritical temperatures. American Mineralogist 86, 1100–1111.

Bohr, C., 1899. Definition und Methode zur Bestimmung der Invasions–und Evasionscoefficienten bei der Auflösung von Gasen in Flüssigkeiten. Werthe der Genannten Constanten Sowie der Absorptionscoefficienten der Kohlensäure bei Auflösung in Wasser und in Chlornatriumlosungen. Annalen der Physik 304, 500–525.

Bohr, C., Bock, J., 1891. Bestimmung der Absorption Einiger Gase in Wasser bei den Temperaturen zwischen 0 und 100 C. Annalen der Physik 280, 318–343.

Briones, J.A., Mullins, J.C., Thies, M.C., Kim, B.U., 1987. Ternary phase equilibria for acetic acid–water mixtures with supercritical carbon dioxide. Fluid Phase Equilibria 36, 235–246.

Bunsen, R.W.E., 1855a. Memoire sur la loi de l'absorption des gaz par les liquides. Annales de Chimie et de Physique 43, 496–508.

Bunsen, R.W.E., 1855b. On the law of absorption of gases. Philosophical Magazine 9 (116–130), 181–201.

Burmakina, G.V., Efanov, L.N., Shnet, M.A., 1982. Solubility of CO_2 in aqueous solutions of electrolytes and of sucrose. Russian Journal of Physical Chemistry 56, 705–707.

Carroll, J.J., Slupsky, J.D., Mather, A.E., 1991. The solubility of carbon dioxide in water at low pressure. Journal of Physical and Chemical Reference Data 20, 1201–1209.

Chapoy, A., Mohammadi, A.H., Chareton, A., Tohidi, B., Richon, D., 2004. Measurement and modeling of gas solubility and literature review of the properties for the carbon dioxide–water system. Industrial and Engineering Chemistry Research 43, 1794–1802.

Coan, C.R., King, A.D.J., 1971. Solubility of water in compressed carbon dioxide, nitrous oxide, and ethane. Evidence for hydration of carbon dioxide and nitrous oxide in the gas phase. Journal of the American Chemical Society 93, 1857–1862.

Cramer, S.D., 1982. The solubility of methane, carbon dioxide, and oxygen in brines from 0 to 300 C: Bureau of Mines Report of Investigations, 8706.

Crovetto, R., 1991. Evaluation of solubility data of the system CO_2-H_2O from 273 K to the critical point of water. Journal of Physical and Chemical Reference Data 20, 575–589.

Crovetto, R., Wood, R.H., 1992. Solubility of CO_2 in water and density of aqueous CO_2 near the solvent critical temperature. Fluid Phase Equilibria 74, 271–288.

Curry, J., Hazelton, C.L., 1938. The solubility of carbon dioxide in deuterium oxide at 25 C. Journal of the American Chemical Society 60, 2771–2773.

Daval, D., Sissmann, O., Menguy, N., Saldi, G.D., Guyot, F., Martinez, I., Corvisier, J., Garcia, B., Machouk, I., Knauss, K.G., Hellmann, R., 2011. Influence of amorphous silica layer formation on the dissolution rate of olivine at 90°C and elevated pCO_2. Chemical Geology 284, 193–209.

de Khanikof, N., Louguinine, V., 1867. Experiences pour verifier la loi de Henry et Dalton sur l'absorption des gaz par les liquides a temperature constante et sous des pressions variables. Annales de Chimie et de Physique 11, 412–433.

Dhima, A., de Hemptinne, J.C., Jose, J., 1999. Solubility of hydrocarbons and CO_2 mixtures in water under high pressure. Industrial and Engineering Chemistry Research 38, 3144–3161.

Diamond, L.W., Akinfiev, N.N., 2003. Solubility of CO_2 in water from −1.5 to 100 C and from 0.1 to 100 MPa: evaluation of literature data and thermodynamic modelling. Fluid Phase Equilibria 208, 265–290.

DiSouza, R., Patrick, J.R., Teja, A.S., 1988. High pressure phase equilibria in the carbon dioxide — n-hexadecane and carbon dioxide–water systems. Canadian Journal of Chemical Engineering 66, 319–323.

Dodds, W.S., Stutzman, L.F., Sollami, B.J., 1956. Carbon dioxide solubility in water. Industrial and Engineering Chemistry Chemical and Engineering Data Series 1, 92–95.

Dohrn, R., Bunz, A.P., Devlieghere, F., Thelen, D., 1993. Experimental measurements of phase equilibria for ternary and quaternary systems of glucose, water, CO_2 and ethanol with a novel apparatus. Fluid Phase Equilibria 83, 149–158.

Drummond, J., S. E., 1981. Boiling and mixing of hydrothermal fluids: Chemical effects on mineral precipitation, PhD thesis, Pennsylvania State University.

Duan, Z.H., Sun, R., 2003. An improved model calculating CO_2 solubility in pure water and aqueous NaCl solutions from 273 to 533 K and from 0 to 2000 bar. Chemical Geology 193, 257–271.

Duan, Z.H., Moller, N., Weare, J.H., 1995. Equation of state for the NaCl-H_2O-CO_2 system — prediction of phase-equilibria and volumetric properties. Geochimica et Cosmochimica Acta 59, 2869–2882.

Duan, Z.H., Moller, N., Weare, J.H., 2003. Equations of state for the NaCl-H_2O-CH_4 system and the NaCl-H_2O-CO_2-CH_4 system: phase equilibria and volumetric properties above 573 K. Geochimica et Cosmochimica Acta 67, 671–680.

Duan, Z.H., Sun, R., Zhu, C., Chou, I.M., 2006. An improved model for the calculation of CO_2 solubility in aqueous solutions containing Na^+, K^+, Ca^{2+}, Mg^{2+}, Cl^-, and SO_4^{2-}. Marine Chemistry 98, 131–139.

Ellis, A.J., 1959. The solubility of carbon dioxide in water at high temperatures. American Journal of Science 257, 217–234.

Ellis, A.J., Golding, R.M., 1963. The solubility of carbon dioxide above 100 C in water and in sodium chloride solutions. American Journal of Science 261, 47–60.

Eremina, A.O., Efanov, L.N., Sorokina, N.A., 1989. Structural transformation in aqueous solutions of electrolytes. Russian Journal of Physical Chemistry 63, 1361–1363.

Fan, S.S., Guo, T.M., 1999. Hydrate formation of CO_2-rich binary and quaternary gas mixtures in aqueous sodium chloride solutions. Journal of Chemical and Engineering Data 44, 829–832.

Felmy, A.R., Qafoku, O., Arey, B.W., Hu, J.Z., Hu, M., Schaef, H.T., Ilton, E.S., Hess, N.J., Pearce, C.I., Feng, J., Rosso, K.M., 2012. Reaction of water-saturated super-critical CO_2 with forsterite: evidence for magnesite formation at low temperatures. Geochimica et Cosmochimica Acta 91, 271–282.

Fenghour, A., Wakeham, W.A., Watson, J.T.R., 1996. Densities of (water + carbon dioxide) in the temperature range 415 K to 700 K and pressures up to 35 MPa. The Journal of Chemical Thermodynamics 28, 433–446.

Findlay, A., Creighton, H.J.M., 1910. The influence of colloids and fine suspensions on the solubility of gases in water. Part I. Solubility of carbon dioxide and nitrous oxide. Journal of the Chemical Society 97, 536–561.

Findlay, A., Howell, O.R., 1915. The solubility of carbon dioxide in water in the presence of starch. Journal of the Chemical Society 107, 282–284.

Findlay, A., Shen, B., 1912. The influence of colloids and fine suspensions on the solubility of gases in water. Part II. Solubility of carbon dioxide and of hydrogen. Journal of the Chemical Society 101, 1459–1468.

Findlay, A., Williams, T., 1913. The influence of colloids and fine suspensions on the solubility of gases in water. Part III. Solubility of carbon dioxide at pressures lower than atmospheric. Journal of the Chemical Society 103, 636–645.

Garcia, B., Beaumont, V., Perfetti, E., Rouchon, V., Blanchet, D., Oger, P., Dromart, G., Huc, A.Y., Haeseler, F., 2010. Experiments and geochemical modelling of CO_2 sequestration by olivine: potential, quantification. Applied Geochemistry 25, 1383–1396.

Garner, F.H., Long, R., Miller, D.G., 1959. Equilibria, at moderate pressures, in the system CO_2, H_2S, N_2 — sodium carbonate, sodium bicarbonate, sodium hydrosulfide and water. Journal of Applied Chemistry 9, 534–542.

Geffcken, G., 1904. Articles on knowledge of solubility influencing. Zeitschrift fur Physikalische Chemie Stochiometrie und Verwandtschaftslehre 49, 257–302.

Gehrig, M., 1980. Phase equilibria and PVT data in the ternary mixture water, carbon dioxide, and sodium chloride to 3 kbar and 550 C, PhD thesis, University Karlsruhe.

Gerecke, J., 1969. Ein Beitrag zur Gaslöslichkeit in Elektrolytlösungen Untersucht am Beispiel der Löslichkeit von H_2, CO_2 und NH_3 in Wasser und Wässrigen Salzlösungen, PhD thesis, Technische Hochschule für Chemie Carl Schorlemmer Leuna Merseburg.

Giammar, D.E., Bruant, R.G., Peters, C.A., 2005. Forsterite dissolution and magnesite precipitation at conditions relevant for deep saline aquifer storage and sequestration of carbon dioxide. Chemical Geology 217, 257–276.

Gillespie, P.C., Owens, J.L., Wilson, G.M., 1984. Sour Water Equilibria Extended to High Temperatures and with Inerts Present. AIChE Winter National Meeting Atlanta, paper 34-b.

Gruszkiewicz, M.S., Palmer, D.A., Springer, R.D., Wang, P.M., Anderko, A., 2007. Phase Behavior of aqueous Na-K-Mg-Ca-Cl-NO_3 mixtures: Isopiestic measurements and thermodynamic modeling. Journal of Solution Chemistry 36, 723–765.

Gurvich, L.V., Veyts, I.V., Alcock, C.B., 1990. Thermodynamic properties of individual substances, 4th ed. Hemisphere Publishing Corporation.

Guyot, F., Daval, D., Dupraz, S., Martinez, I., Menez, B., Sissmann, O., 2011. CO_2 geological storage: the environmental mineralogy perspective. Comptes Rendus Geoscience 343, 246–259.

Haar, L., Gallagher, J.S., Kell, G.S., 1984. NBS/NRC steam tables: thermodynamic and transport properties and computer programs for vapor and liquid states in SI units. Hemisphere Publishing, Washington, DC.

Hanchen, M., Prigiobbe, V., Storti, G., Seward, T.M., Mazzotti, M., 2006. Dissolution kinetics of fosteritic olivine at 90–150°C including effects of the presence of CO_2. Geochimica et Cosmochimica Acta 70, 4403–4416.

Hanchen, M., Prigiobbe, V., Baciocchi, R., Mazzotti, M., 2008. Precipitation in the Mg-carbonate system — effects of temperature and CO_2 pressure. Chemical Engineering Science 63, 1012–1028.

Hantzsch, A., Vogt, A., 1901. On the state of soluble materials on the basis of spacing tests. Zeitschrift fur Physikalische Chemie Stochiometrie und Verwandtschaftslehre 38, 705–742.

Harned, H.S., Davis Jr., R., 1943. The ionization constant of carbonic acid in water and the solubility of carbon dioxide in water and aqueous salt solutions from 0 to 50 C. Journal of the American Chemical Society 65, 2030–2037.

Harvey, A.H., Prausnitz, J.M., 1989. Thermodynamics of high-pressure aqueous systems containing gases and salts. AICHE Journal 35, 635–644.

Hayduk, W., Malik, V.K., 1971. Density, viscosity, and carbon dioxide solubility and diffusivity in aqueous ethylene glycol solutions. Journal of Chemical and Engineering Data 16, 143–146.

He, S.L., Morse, J.W., 1993. The carbonic acid system and calcite solubility in aqueous Na-K-Ca-Mg-Cl-SO_4 solutions from 0 to 90 C. Geochimica et Cosmochimica Acta 57, 3533–3554.

Helgeson, H.C., Kirkham, D.H., Flowers, G.C., 1974a. Theoretical prediction of the thermodynamic behavior of aqueous electrolytes at high pressures and temperatures. I Summary of the thermodynamic/electrostatic properties of the solvent. American Journal of Science 274, 1089–1198.

Helgeson, H.C., Kirkham, D.H., Flowers, G.C., 1974b. Theoretical prediction of the thermodynamic behavior of aqueous electrolytes at high pressures and temperatures. II Debye–Hűckel parameters for activity coefficients and relative partial molal properties. American Journal of Science 274, 1199–1261.

Helgeson, H.C., Kirkham, D.H., Flowers, G.C., 1976. Theoretical prediction of the thermodynamic behavior of aqueous electrolytes at high pressures and temperatures. III Equation of state for aqueous species at infinite dilution. American Journal of Science 276, 97–240.

Helgeson, H.C., Kirkham, D.H., Flowers, G.C., 1981. Theoretical prediction of the thermodynamic behavior of aqueous electrolytes at high pressures and temperatures. IV. Calculation of activity coefficients, osmotic coefficients, and apparent molal and standard and relative partial molal properties to 5 kb and 600°C. American Journal of Science 281.

Houghton, G., McLean, A.M., Ritchie, P.D., 1957. Compressibility, fugacity, and water solubility of carbon dioxide in the region 0–36 atm and 0–100 C. Chemical Engineering Science 6, 132–137.

Jackson, K., Bowman, L.E., Fulton, J.L., 1995. Water solubility measurements in supercritical fluids and high-pressure liquids using near-infrared spectroscopy. Analytical Chemistry 67, 2368–2372.

Ji, X.Y., Tan, S.P., Adidharma, H., Radosz, M., 2005. SAFT1-RPM approximation extended to phase equilibria and densities of CO_2-H_2O and CO_2-H_2O-NaCl systems. Industrial and Engineering Chemistry Research 44, 8419–8427.

Jin, G., Donohue, M.D., 1988. An equation of state for electrolyte solutions. 2. Single volatile weak electrolytes in water. Industrial and Engineering Chemistry Research 27, 1737–1743.

Johnson, J.W., Oelkers, E.H., Helgeson, H.C., 1992. SUPCRT92 — a software package for calculating the standard molal thermodynamic properties of minerals, gases, aqueous species, and reactions from 1 bar to 5000 bar and 0 °C to 1000 °C. Computers & Geosciences 18, 899–947.

Kamps, A.P.S., Meyer, E., Rumpf, B., Maurer, G., 2007. Solubility of CO_2 in aqueous solutions of KCl and in aqueous solutions of K_2CO_3. Journal of Chemical and Engineering Data 52, 817–832.

Kiepe, J., Horstmann, S., Fischer, K., Gmehling, J., 2002. Experimental determination and prediction of gas solubility data for CO_2 + H_2O mixtures containing NaCl or KCl at temperatures between 313 and 393 K and pressures up to 10 MPa. Industrial and Engineering Chemistry Research 41, 4393–4398.

King, M.B., Mubarak, A., Kim, J.D., Bott, T.R., 1992. The mutual solubilities of water with supercritical and liquid carbon dioxide. Journal of Supercritical Fluids 5, 296–302.

King, H.E., Plumper, O., Putnis, A., 2010. Effect of secondary phase formation on the carbonation of olivine. Environmental Science & Technology 44, 6503–6509.

Kobe, K.A., Williams, J.S., 1935. Confining liquids for gas analysis. Solubility of carbon dioxide in salt solutions. Industrial and Engineering Chemistry, Analytical Edition 7, 37–38.

Koch Jr., H.A., Stutzman, L.F., Blum, H.A., Hutchings, L.E., 1949. Gas absorption. Liquid transfer coefficients for the carbon dioxide–air–water system. Chemical Engineering Progress 45, 677–682.

Koschel, D., Coxam, J.Y., Rodier, L., Majer, V., 2006. Enthalpy and solubility data of CO_2 in water and NaCl(aq) at conditions of interest for geological sequestration. Fluid Phase Equilibria 247, 107–120.

Kosinski, J.J., Wang, P.M., Springer, R.D., Anderko, A., 2007. Modeling acid-base equilibria and phase behavior in mixed-solvent electrolyte systerns. Fluid Phase Equilibria 256, 34–41.

Kritschewski, I.R., Shaworonkoff, N.M., Aepelbaum, V.A., 1935. Combined solubility of gases in liquids under pressure. I. Solubility of carbon dioxide in water from its mixtures with hydrogen of 20 and 30 C and total pressure of 30 kg/cm^2. Zeitschrift für Physikalische Chemie Abteilung A 175, 232–238.

Kunerth, W., 1922. Solubility of CO_2 and N_2O in certain solvents. Physical Review 19, 512–524.

Kwak, J.H., Hu, J.Z., Hoyt, D.W., Sears, J.A., Wang, C.M., Rosso, K.M., Felmy, A.R., 2010. Metal carbonation of forsterite in supercritical CO_2 and H_2O using solid state Si-29, C-13 NMR spectroscopy. Journal of Physical Chemistry C 114, 4126–4134.

Kwak, J.H., Hu, J.Z., Turcu, R.V.F., Rosso, K.M., Ilton, E.S., Wang, C., Sears, J.A., Engelhard, M.H., Felmy, A.R., Hoyt, D.W., 2011. The role of H_2O in the carbonation of forsterite in supercritical CO_2. International Journal of Greenhouse Gas Control 5, 1081–1092.

Li, D., Duan, Z., 2007. The speciation equilibrium coupling with phase equilibrium in the H_2O-CO_2-NaCl system from 0 to 250 C, from 0 to 1000 bar, and from 0 to 5 molality of NaCl. Chemical Geology 244, 730–751.

Li, J., Duan, Z., 2011. A thermodynamic model for the prediction of phase equilibria and speciation in the H_2O-CO_2-NaCl-$CaCO_3$-$CaSO_4$ system from 0 to 250 degrees C, 1 to 1000 bar with NaCl concentrations up to halite saturation. Geochimica et Cosmochimica Acta 75, 4351–4376.

Li, Y.K., Nghiem, L.X., 1986. Phase equilibria of oil, gas and water brine mixtures from a cubic equation of state and Henry law. Canadian Journal of Chemical Engineering 64, 486–496.

Li, Y.H., Tsui, T.F., 1971. Solubility of CO_2 in water and sea water. Journal of Geophysical Research 76, 4203–4207.

Li, J.D., Topphoff, M., Fischer, K., Gmehling, J., 2001. Prediction of gas solubilities in aqueous electrolyte systems using the predictive Soave–Redlich–Kwong model. Industrial and Engineering Chemistry Research 40, 3703–3710.

Li, Z., Dong, M., Li, S., Dai, L., 2004. Densities and solubilities for binary systems of carbon dioxide + water and carbon dioxide + brine at 59 C and pressures to 29 MPa. Journal of Chemical and Engineering Data 49, 1026–1031.

Lin, Y., Thomsen, K., de Hemptinne, J.C., 2007. Multicomponent equations of state for electrolytes. AICHE Journal 53, 989–1005.

Lin, H., Fujii, T., Takisawa, R., Takahashi, T., Hashida, T., 2008. Experimental evaluation of interactions in supercritical CO_2/water/rock minerals system under geologic CO_2 sequestration conditions. Journal of Materials Science 43, 2307–2315.

Loring, J.S., Thompson, C.J., Wang, Z.M., Joly, A.G., Sklarew, D.S., Schaef, H.T., Ilton, E.S., Rosso, K.M., Felmy, A.R., 2011. In situ infrared spectroscopic study of forsterite carbonation in wet supercritical CO_2. Environmental Science & Technology 45, 6204–6210.

Mackenzie, J.J., 1877. Über die Absorption der Gase durch Salzlösungen. Annalen der Physik 237, 438–451.

Mäder, U.K., 1991. H_2O-CO_2 mixtures — a review of P–V–T–X data and an assessment from a phase equilibrium point of view. The Canadian Mineralogist 29, 767–790.

Malinin, S.D., 1959. The system water — carbon dioxide at high temperatures and pressures. Geochemistry 3, 292–306.

Malinin, S.D., Kurovskaya, N.A., 1975. Solubility of CO_2 in chloride solutions at elevated temperatures and CO_2 pressures. Geochemistry International 12, 199–201.

Malinin, S.D., Savelyeva, N.I., 1972. Experimental investigations of CO_2 solubility in NaCl and $CaCl_2$ solutions at temperatures of 25, 50 and 75 C and elevated CO_2 pressure. Geochemistry International 9, 410–418.

Markham, A.E., Kobe, K.A., 1941. The solubility of carbon dioxide and nitrous oxide in aqueous salt solutions. Journal of the American Chemical Society 63, 449–454.

Mather, A.E., Franck, E.U., 1992. Phase equilibria in the system carbon dioxide–water at elevated pressures. Journal of Physical Chemistry 96, 6–8.

Matous, J., Sobr, J., Novak, J.P., Pick, J., 1969. Solubility of carbon dioxide in water at pressures up to 40 atm. Collection of Czechoslovak Chemical Communications 34, 3982–3985.

McGrail, B.P., Schaef, H.T., Glezakou, V.A., Dang, L.X., Owen, A.T., 2009. Water reactivity in the liquid and supercritical CO_2 phase: Has half the story been neglected? In: Gale, J., Herzog, H., Braitsch, J. (Eds.), Greenhouse Gas Control Technologies, p. 9.
Morgan, O.M., Maass, O., 1931. An investigation of the equilibria existing in gas–water systems forming electrolytes. Canadian Journal of Research 5, 162–199.
Morgan, J.L.R., Pyne, H.R., 1930. Solubility relations in gas–liquid systems. I. A new apparatus for determining gas solubilities. Journal of Physical Chemistry 34, 1578–1582.
Morrison, T.J., Billett, F., 1952. The salting-out of non-electrolytes. Part II. The effect of variation in non-electrolyte. Journal of the Chemical Society 3819–3822.
Müller, G., Bender, E., Maurer, G., 1988. Vapor liquid equilibrium in the ternary system ammonia–carbon dioxide–water at high water contents in the range 373 K to 473 K. Berichte der Bunsengesellschaft für Physikalische Chemie 92, 148–160.
Murray, C.N., Riley, J.P., 1971. The solubility of gases in distilled water and sea water: IV. Carbon dioxide. Deep Sea Research 18, 533–541.
Nakayama, T., Sagara, H., Arai, K., Saito, S., 1987. High pressure liquid–liquid equilibria for the system of water, ethanol and 1,1-difluoroethane at 323.2 K. Fluid Phase Equilibria 38, 109–127.
Nighswander, J.A., Kalogerakis, N., Mehrotra, A.K., 1989. Solubilities of carbon dioxide in water and 1 wt% NaCl solution at pressures up to 10 MPa and temperatures from 80 to 200 C. Journal of Chemical and Engineering Data 34, 355–360.
Nordbotten, J.M., Celia, M.A., 2006. Similarity solutions for fluid injection into confined aquifers. Journal of Fluid Mechanics 561, 307–327.
Novak, J., Fried, V., Pick, J., 1961. Löslichkeit des Kohlendioxyds in Wasser bei Verschiedenen Drücken und Temperaturen. Collection of Czechoslovak Chemical Communications 26, 2266–2270.
Ohgaki, K., Makihara, Y., Takano, K., 1993. Formation of CO_2 hydrate in pure and sea waters. Journal of Chemical Engineering of Japan 26, 558–564.
OLISystems, 2012. OLI Software: Stream Analyzer and ESP (Electrolyte Simulation Program), version 9.0.
Onda, K., Sada, E., Kobayashi, T., Kito, S., Ito, K., 1970a. Salting-out parameters of gas solubility in aqueous salt solutions. Journal of Chemical Engineering of Japan 3, 18–24.
Onda, K., Sada, E., Kobayashi, T., Kito, S., Ito, K., 1970b. Solubility of gases in aqueous solutions of mixed salts. Journal of Chemical Engineering of Japan 3, 137–142.
Oyevaar, M.H., Morssinkhof, R.W.J., Westerterp, K.R., 1989. Density, viscosity, solubility, and diffusivity of CO_2 and N_2O in solutions of diethanolamine in aqueous ethylene glycol at 298 K. Journal of Chemical and Engineering Data 34, 77–82.
Pitzer, K.S., 1973. Thermodynamics of electrolytes. I. Theoretical basis and general equations. Journal of Physical Chemistry 77, 268–277.
Pitzer, K.S., 1980. Electrolytes — from dilute solutions to fused salts. Journal of the American Chemical Society 102, 2902–2906.
Pitzer, K.S., 1995. Thermodynamics, 3rd edition. McGraw-Hill, New York.
Postigo, M.A., Katz, M., 1987. Solubility and thermodynamics of carbon dioxide in aqueous ethanol solutions. Journal of Solution Chemistry 16, 1015–1024.
Power, G.G., Stegall, H., 1970. Solubility of gases in human red blood cell ghosts. Journal of Applied Physiology 29, 145–149.
Prigiobbe, V., Costa, G., Baciocchi, R., Hanchen, M., Mazzotti, M., 2009. The effect of CO_2 and salinity on olivine dissolution kinetics at 120°C. Chemical Engineering Science 64, 3510–3515.
Prutton, C.F., Savage, R.L., 1945. The solubility of carbon dioxide in calcium chloride–water solutions at 75, 100, 120 C and high pressures. Journal of the American Chemical Society 67, 1550–1554.
Prytz, K., Holst, H., 1895. Die Absorptionscoefficienten der Kohlensäure und des Schweffelwasserstoffs in Wasser bei dessen Gefrierpunkt. Annalen der Physik 290, 130–139.
Rafal, M., Berthold, J.W., Scrivner, N.C., Grise, S.L., 1995. Models for Electrolyte Solutions. In: Sandler, S.I. (Ed.), Models for Thermodynamic and Phase Equilibria Calculations. Marcel Dekker, New York.
Regnault, O., Lagneau, V., Catalette, H., Schneider, H., 2005. Experimental study of pure mineral phases/supercritical CO_2 reactivity. Implications for geological CO_2 sequestration. Comptes Rendus Geoscience 337, 1331–1339.
Robie, R.A., Hemingway, B.S., 1995. Thermodynamic properties of minerals and related substances at 298.15 K and 1 bar (10^5 Pa) pressure and at higher temperatures. U.S. Geological Survey Bulletin 2131, 461.
Rosenthal, W., 1954. Contribution a l'étude de la solubilité des gaz dans quelques solvants et solutions, PhD thesis, University Strasbourg, France.
Rumpf, B., Nicolaisen, H., Ocal, C., Maurer, G., 1994. Solubility of carbon dioxide in aqueous solutions of sodium chloride: experimental results and correlation. Journal of Solution Chemistry 23, 431–448.
Sako, T., Sugeta, T., Nakazawa, N., Okubo, T., Sato, M., Taguchi, T., Hiaki, T., 1991. Phase equilibrium study of extraction and concentration of furfural produced in reactor using supercritical carbon dioxide. Journal of Chemical Engineering of Japan 24, 449–455.
Salari, H., Hassanzadeh, H., Gerami, S., Abedi, J., 2011. On estimating the water content of CO_2 in equilibrium with formation brine. Petroleum Science and Technology 29, 2037–2051.
Sander, W., 1912. On the solubility of carbon acid in water and some other solutions under high pressure. Zeitschrift für Physikalische Chemie Stochiometrie und Verwandtschaftslehre 78, 513–549.
Scharlin, P., 1996. Carbon dioxide in water and aqueous electrolyte solutions, IUPAC Solubility Data Series 62. Pergamon Press.
Servio, P., Englezos, P., 2001. Effect of temperature and pressure on the solubility of carbon dioxide in water in the presence of gas hydrate. Fluid Phase Equilibria 190, 127–134.
Setchenow, J., 1879. Mémoires de l'Academie Imperiale des Sciences de Saint-Petersbourg 7th Series 26, 1–62.
Setchenow, J., 1887. Mémoires de l'Academie Imperiale des Sciences de Saint-Petersbourg 7th Series 35, 1–59.
Setchenow, J., 1889. Mosk. Obsh. Spyt. Prirody. Nouveaux Mémoires de la Société Impériale des Naturalistes de Moscou 15, 203–274.
Setchenow, J., 1892. Action de l'acide carbonique sur les solutions des sels a acides forts. Etude absorptiometrique. Annales de Chimie et de Physique 25, 226–270.
Setschenow, S., 1874. Über die Absorptiometrie in Ihrer Anwendung auf die Zustände der Kohlensäure im Blute. Pflügers Archiv 8, 1–39.
Shagiakhmetov, R.A., Tarzimanov, A.A., 1981. Measurements of CO_2 solubility in water up to 60 MPa. Deposited Document SPSTL 200khp D81, cited in Scharlin (1996).
Shchennikova, M.K., Devyatykh, G.G., Korshunov, I.A., 1957. Russian Journal of Applied Chemistry 30, 881–886.
Shedlovsky, T., MacInnes, D.A., 1935. The first ionization constant of carbonic acid, 0 to 38 C, from conductance measurements. Journal of the American Chemical Society 57, 1705–1710.
Shock, E.L., Helgeson, H.C., 1988. Calculation of the thermodynamic and transport properties of aqueous species at high pressures and temperatures: Correlation algorithms for ionic species and equation of state predictions to 5 kb and 1000°C. Geochimica et Cosmochimica Acta 52, 2009–2036.
Shock, E.L., Helgeson, H.C., Sverjensky, D.A., 1989. Calculation of the thermodynamic and transport properties of species at high pressures and temperatures: Standard partial molar properties of inorganic neutral species. Geochimica et Cosmochimica Acta 53, 2157–2183.
Soave, G., 1972. Equilibrium constants from a modified Redlich-Kwong equation of state. Chemical Engineering Science 27, 1197-&.
Spycher, N., Pruess, K., 2005. CO_2-H_2O mixtures in the geological sequestration of CO_2. II. Partitioning in chloride brines at 12-100 C and up to 600 bar. Geochimica et Cosmochimica Acta 69, 3309–3320.
Spycher, N., Pruess, K., Ennis-King, J., 2003. CO_2-H_2O mixtures in the geological sequestration of CO_2. I. Assessment and calculation of mutual solubilities from 12 to 100 C and up to 600 bar. Geochimica et Cosmochimica Acta 67, 3015–3031.
Sterner, S.M., Bodnar, R.J., 1991. Synthetic fluid inclusions. X: Experimental determination of P–V–T–X properties in the CO_2–H_2O system to 6 kb and 700 C. American Journal of Science 291, 1–54.
Stewart, P.B., Munjal, P., 1970. Solubility of carbon dioxide in pure water, synthetic sea water, and synthetic sea water concentrates at -5 to 25 C and 10 to 45 atm pressure. Journal of Chemical and Engineering Data 15, 67–71.
Stone, H.W., 1943. Solubility of water in liquid carbon dioxide. Industrial and Engineering Chemistry 35, 1284–1286.
Suto, Y., Liu, L.H., Yamasaki, N., Hashida, T., 2007. Initial behavior of granite in response to injection of CO_2-saturated fluid. Applied Geochemistry 22, 202–218.
Takenouchi, S., Kennedy, G.C., 1964. The binary system H_2O–CO_2 at high temperatures and pressures. American Journal of Science 262, 1055–1074.
Takenouchi, S., Kennedy, G.C., 1965. The solubility of carbon dioxide in NaCl solutions at high temperatures and pressures. American Journal of Science 263, 445–454.
Tan, S.P., Adidharma, H., Radosz, M., 2008. Recent advances and applications of Statistical Associating Fluid Theory. Industrial and Engineering Chemistry Research 47, 8063–8082.
Tanger, J.C., Helgeson, H.C., 1988. Calculation of the thermodynamic and transport properties of aqueous species at high pressures and temperatures: revised equations of state for the standard partial molal properties of ions and electrolytes. American Journal of Science 288, 19–98.
Teng, H., Yamasaki, A., Chun, M.K., Lee, H., 1997. Solubility of liquid CO_2 in water at temperatures from 278 K to 293 K and pressures from 6.44 MPa to 29.49 MPa and densities of the corresponding aqueous solutions. The Journal of Chemical Thermodynamics 29, 1301–1310.
Tödheide, K., Franck, E.U., 1963. Das Zweiphasengebeit und die Kritische Kurve im System Kohlendioxid - Wasser bis zu Drucken von 3500 bar. Zeitschrift fur Physikalische Chemie Frankfurt 37, 387–401.
Traub, P., Stephan, K., 1990. High-pressure phase equilibria of the system CO_2–water–acetone measured with a new apparatus. Chemical Engineering Science 45, 751–758.
TRC, 1989. TRC Thermodynamics Tables — Non-hydrocarbons. Thermodynamic Research Center, The Texas A & M University System, College Station, TX.
Valtz, A., Chapoy, A., Coquelet, C., Paricaud, P., Richon, D., 2004. Vapor–liquid equilibria in the carbon dioxide–water system, measurement and modeling from 278.2 to 318.2 K. Fluid Phase Equilibria 226, 333–344.
Van Slyke, D.D., 1939. Determination of solubilities of gases in liquids with use of the Van Slyke–Neill manometric apparatus for both saturation and analysis. Journal of Biological Chemistry 130, 545–554.
Vazquez, G., Chenlo, F., Pereira, G., 1994a. CO_2 diffusivity in NaCl and $CuSO_4$ aqueous solutions. Afinidad 51, 369–374.
Vazquez, G., Chenlo, F., Pereira, G., Peaguda, J., 1994b. Solubility of CO_2 in aqueous solutions of NaCl, $CuSO_4$, KI and NaBr. Anales de Quimica 90, 324–328.
Vilcu, R., Gainar, I., 1967. Löslichkeit der Gase unter Druck in Flüssigkeiten I. Das System Kohlendioxid - Wasser. Revue Roumaine de Chimie 12, 181–189.
Wagman, D.D., Evans, W.H., Parker, V.B., Schumm, R.H., Halow, I., Bailey, S., Churney, K.L., Nuttal, R.L., 1982. The NBS tables of chemical thermodynamic properties. Selected values for inorganic and C1 and C2 organic substances in SI units, Supplement 2. Journal of Physical and Chemical Reference Data 11, 2–392.
Wang, P.M., Anderko, A., Young, R.D., 2002. A speciation-based model for mixed-solvent electrolyte systems. Fluid Phase Equilibria 203, 141–176.
Wang, P., Springer, R.D., Anderko, A., Young, R.D., 2004. Modeling phase equilibria and speciation in mixed-solvent electrolyte systems. Fluid Phase Equilibria 222, 11–17.
Wang, P., Anderko, A., Springer, R.D., Young, R.D., 2006. Modeling phase equilibria and speciation in mixed-solvent electrolyte systems: II. Liquid–liquid equilibria and properties of associating electrolyte solutions. Journal of Molecular Liquids 125, 37–44.

Wang, P.M., Anderko, A., Springer, R.D., Kosinski, J.J., Lencka, M.M., 2010. Modeling chemical and phase equilibria in geochemical systems using a speciation-based model. Journal of Geochemical Exploration 106, 219–225.
Wendland, M., Hasse, H., Maurer, G., 1999. Experimental pressure–temperature data on three- and four-phase equilibria of fluid, hydrate, and ice phases in the system carbon dioxide–water. Journal of Chemical and Engineering Data 44, 901–906.
Wiebe, R., Gaddy, V.L., 1939. The solubility in water of carbon dioxide at 50, 75 and 100C, at pressures to 700 atmospheres. Journal of the American Chemical Society 61, 315–318.
Wiebe, R., Gaddy, V.L., 1940. Solubility of carbon dioxide in water at various temperatures from 12 to 40C and at pressures to 500 atmospheres. Critical phenomena. Journal of the American Chemical Society 62, 815–817.
Wiebe, R., Gaddy, V.L., 1941. Vapor phase composition of carbon dioxide–water mixtures at various temperatures and at pressures to 700 atmospheres. Journal of the American Chemical Society 63, 475–477.
Won, Y.S., Chung, D.K., Mills, A.F., 1981. Density, viscosity, surface tension, and carbon dioxide solubility and diffusivity of methanol, ethanol, aqueous propanol, and aqueous ethylene glycol at 25 C. Journal of Chemical and Engineering Data 26, 140–141.
Yang, J.Z., Yuan, C.B., 1993. Thermodynamics of carbonate in aqueous glucose solution. 1. The system of CO_2–$NaHCO_3$–NaCl–glucose–H_2O. Acta Chimica Sinica 51, 849–853.
Yasunishi, A., Yoshida, F., 1979. Solubility of carbon dioxide in aqueous electrolyte solutions. Journal of Chemical and Engineering Data 24, 11–14.
Yasunishi, A., Tsuji, M., Sada, E., 1979. Solubility of carbon dioxide in aqueous mixed-salt solutions. Advances in Chemistry Series Thermodynamic Behavior of Electrolytes in Mixed Solvents II 177, 189–203.
Yeh, S.Y., Peterson, R.E., 1964. Solubility of carbon dioxide, krypton, and xenon in aqueous solution. Journal of Pharmaceutical Sciences 53, 822–824.
Zawisza, A., Malesińska, B., 1981. Solubility of carbon dioxide in liquid water and of water in gaseous carbon dioxide in the range 0.2–5 MPa and at temperatures up to 473 K. Journal of Chemical and Engineering Data 26, 388–391.
Zelvenskii, Y.D., 1937. The solubility of carbon dioxide under pressure. Soviet Chemical Industry 14, 1250–1257.
Zemaitis, J.F.J., Clark, D.M., Rafal, M., Scrivner, N.C., 1986. Handbook of Aqueous Electrolyte Thermodynamics. American Institute of Chemical Engineers, New York, NY.
Zhao, L., Sang, L.Q., Chen, J., Ji, J.F., Teng, H.H., 2010. Aqueous carbonation of natural brucite: relevance to CO_2 sequestration. Environmental Science & Technology 44, 406–411.
Zheng, D.Q., Guo, T.M., Knapp, H., 1997. Experimental and modeling studies on the solubility of CO_2, $CHClF_2$, CHF_3, $C_2H_2F_4$ and $C_2H_4F_2$ in water and aqueous NaCl solutions under low pressures. Fluid Phase Equilibria 129, 197–209.